

IX CHAPTER : SUSTAINABILITY AND HYDROGEN

IX.1	Introduction	2
IX.2	Hydrogen Storage	7
	IX.2.1 High pressure gas cylinders	9
	IX.2.2 Liquid hydrogen	11
	IX.2.3 Physisorption of hydrogen	14
	IX.2.4 Metalhydrides	19
	IX.2.5 Complex hydrides	26
	IX.2.6 Chemical reaction with water	28
	IX.2.7 Summary hydrogen storage	28
IX.3	Energy conversion	30
IX.4	Visions for the Future	33
IX.5	Conclusion	33
IX.6	References	33

Although fossil fuels and nuclear power generation will remain the main energy sources for many more years, there is increasing awareness that sustainability is one of the most important challenges for mankind in the near future. Sustainability involves necessarily renewable energy sources and, consequently, new energy production, storage and distribution scenarios.

The inherently intermittent nature of renewable energy sources renders buffering and storage of energy indispensable. At present energy buffering is mainly provided by fossil fuel-generated electricity. This is not possible when intermittent sources represent more than 30% of the total energy sources. It is therefore necessary to look for other energy carriers. Hydrogen is in this context one of the most attractive candidates since it can be integrated in a clean hydrogen-water-hydrogen closed material loop and offers interesting storage and distribution possibilities. Through electrolysis and fuel cells it can also be linked to the other clean energy carrier: electricity.

Hydrogen exhibits the highest heating value of all chemical fuels. Furthermore, hydrogen is regenerative and environment friendly. For mobile and in many cases also for stationary applications the volumetric and gravimetric density of hydrogen in a storage material is crucial.

Hydrogen can be stored by six different ways:

- in high pressure gas cylinders (up to 800 bar),
- as liquid hydrogen in cryogenic tanks (at 21 K),
- as adsorbed hydrogen on materials with a large specific surface area (at $T < 100$ K),
- as absorbed on interstitial sites in a host metal (at ambient pressure and temperature),
- chemically bond in covalent and ionic compounds (at ambient pressure), or through oxidation of reactive metals e.g. Li, Na, Mg, Al, Zn with water.

The various hydrogen storage systems are reviewed and compared and the physical limitations of each system are outlined.

Before a **sustainable hydrogen economy** can become reality, many knowledge gaps need to be bridged. There exist many technical problems, which are connected to the production of hydrogen (both from fossil and sustainable sources), the clean separation of hydrogen from production gas mixtures, the storage of hydrogen and its transport. Besides these technological problems there are also important economic and societal questions concerning for example the management of energy systems, the public risk perception of a hydrogen based economy, and the need of safety systems.

IX.1 INTRODUCTION

For a long period human beings developed on Earth using only plants, i.e. biomass, as the only energy carrier. The average power consumed by a human body at rest is 0.1 kW and approximately 0.4 kW for a hard working body, delivering about 0.1 kW of work. The consumption of plants did not change the environment because the carbon dioxide liberated by humans and animals, was reabsorbed by the plants in the photosynthesis process. In 1792 Thomas Newcomen discovered the steam engine [1]. For the first time a machine worked for human beings and provided the foundation for an industrialized society. The energy for the steam engine was found in the form of mineral coal, i.e. solar energy stored in the Earth crust over millions of years.

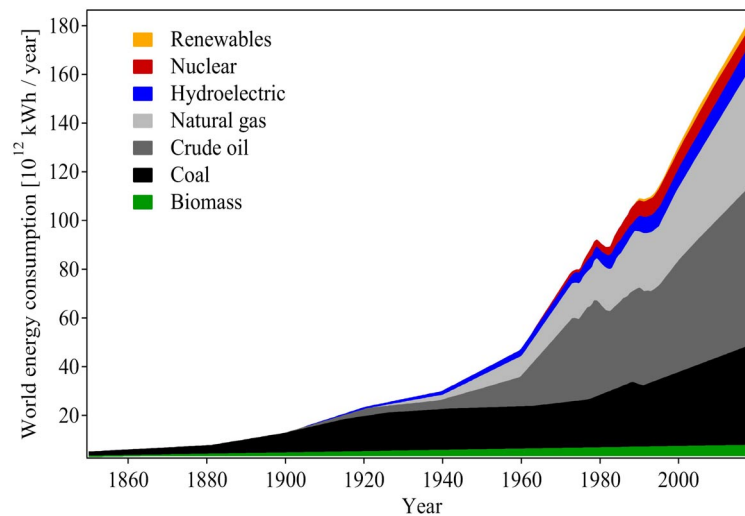


Fig. IX.1: Development of the world energy consumption between 1850 and 2020. More than 80% are based on fossil fuels.

This energy was for free, in the sense that one only had to pay for the mining. Coal, as a solid energy carrier, was later on complemented by liquid crude oil and natural gas. Not only did the state of the energy carrier change with time but also the amount of hydrogen in the fuel increased. As shown in Fig. IX.1 the world energy consumption increased from 5×10^{12} kWh/year in 1860 to 1.4×10^{14} kWh/year today. More than 1.2×10^{14} kWh/year (80%) are based on fossil fuels (coal, oil and gas).

The world population has increased in the last century by a factor of 6 but the energy consumption by a factor of 80 [2]. The worldwide average continuous power consumption today is 2 kW/person. In the USA the power consumption is in average 10 kW/person and in Europe about 5 kW/person. Two billion people on Earth do not consume any fossil fuels at all! The reserves of fossil fuels on Earth are limited and predictions based on the continuation of the energy consumption development show that the demand will soon exceed the supply. Furthermore, the consumption of fossil fuels is responsible for the increase of the carbon dioxide in the atmosphere at a rate of approximately 3×10^{12} kg/year [3].

Carbon dioxide is a greenhouse gas and causes an increase of the average temperature on Earth. The major problem is that a large amount (approximately 98%) of carbon-dioxide on Earth is dissolved in the water of the oceans (7.5×10^{14} kg in the atmosphere, 4.1×10^{16} kg in the ocean). The solubility of carbon dioxide in water decreases with increasing temperature by approximately 3%/K. If the average temperature of the oceans increases the carbon dioxide solubility equilibrium between atmosphere and ocean shifts towards the atmosphere and leads to an additional increase of the greenhouse gas in the atmosphere. This is a positive feedback loop with grave consequences. In the last century there is a clear temperature increase of the Earth (see Fig. IX.3).

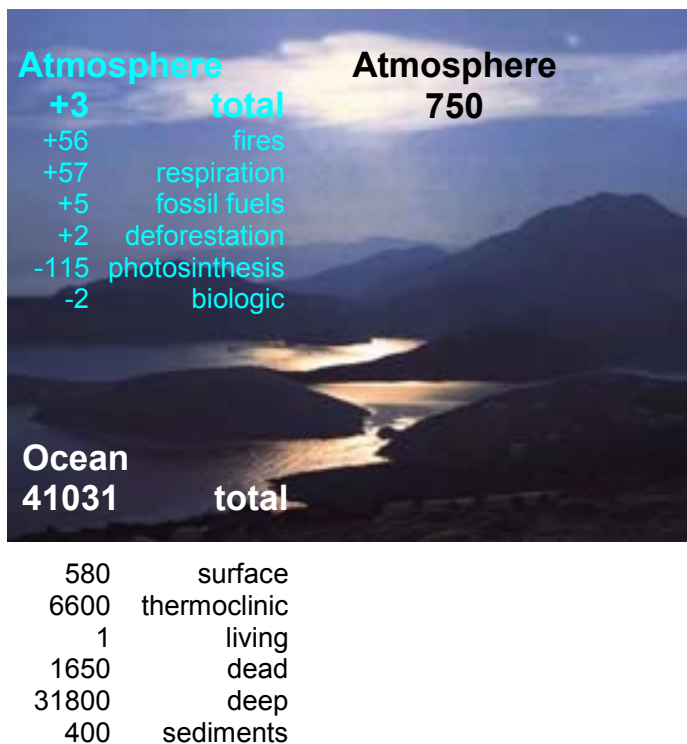


Fig. IX.2: CO₂ reservoirs [in units of 10¹² kg] and sources [in units of 10¹² kg/year] on Earth. The overall change of CO₂ in the atmosphere is +3×10¹² kg/year

On the basis of the historical shift of the energy carriers towards more hydrogen rich fuels and the necessity to avoid carbon dioxide emission, it is natural to expect hydrogen to be **the** energy carrier of the future:

C (coal) → -CH₂- (oil) → CH₄ (natural gas) → H₂ (hydrogen)

This series also shows a development going from a solid (coal) to a liquid (natural gas) and then finally to a gas state energy carrier (hydrogen). Hydrogen is the most abundant element on Earth, however, less than 1% is present as molecular hydrogen gas H₂, the overwhelming part being chemically bound as H₂O in water and to liquid or gaseous hydrocarbons. The production of hydrogen by means of electrolysis consumes electricity, which is often generated in thermal plants. Due to the limitations of the Carnot cycle, only approximately one third of heat can be

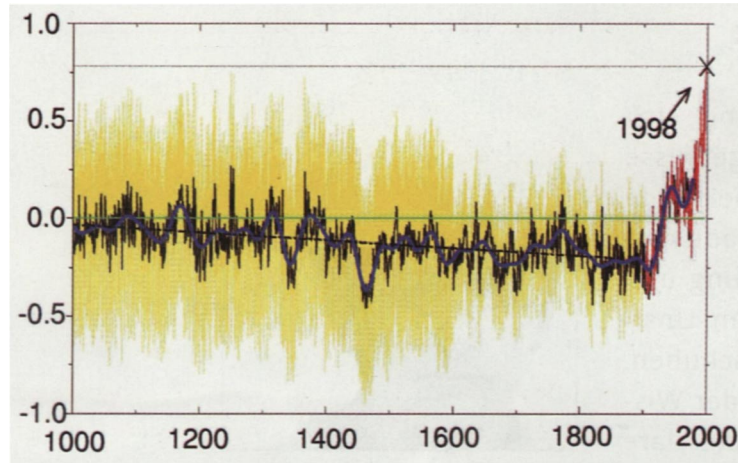


Fig. IX.3: Average temperature change on Earth during the last 1000 years. Ref.: Mann et al., *Geophys. Res. Letters* 26 (1999), pp. 759. After a long steady cooling period during 900 years there is a sharp increase that correlates with the increase of CO_2 in the atmosphere.

converted into work. This implies that energy stored in the form of hydrogen is about three times more expensive than in the form of oil [4].

Chemical energy is based on the energy of unpaired outer electrons (valence electrons) which are to be stabilized by electrons from other atoms. The hydrogen atom is attractive because its electron (for charge neutrality) is accompanied by only one proton, i.e. hydrogen has the highest ratio of valence electrons to protons (and neutrons) and one of the highest ionisation energy of all the elements in the Periodic Table. The chemical energy (higher heating value) per mass of hydrogen (39.4 kWh kg^{-1}) is three times larger than that of other chemical fuels, e.g. liquid hydrocarbons (13.1 kWh kg^{-1}) (see Table IX.1) [5].

Table IX.1: Properties of the fuels hydrogen, methane (natural gas) and gasoline.

Properties		Hydrogen	Methane	Gasoline
		H_2	CH_4	$(-\text{CH}_2-)_n$
lower heating value	$[\text{kWh kg}^{-1}]$	33.33	13.9	12.4
self ignition temperature	$[\text{°C}]$	585	540	228-501
flame temperature	$[\text{°C}]$	2045	1875	2200
ignition limits in air	$[\text{Vol}\%]$	4 - 75	5.3 - 15	1.0 - 7.6
min. ignition energy	$[\text{mWs}]$	0.02	0.29	0.24
flame propagation in air	$[\text{m s}^{-1}]$	2.65	0.4	0.4
detonation limits	$[\text{Vol}\%]$	13 - 65	6.3 - 13.5	1.1 - 3.3
detonation velocity	$[\text{km s}^{-1}]$	1.48 - 2.15	1.39 - 1.64	1.4 - 1.7
explosion energy	$[\text{kg TNT} \cdot \text{m}^{-3}]$	2.02	7.03	44.22
diffusion coef. in air	$[\text{cm}^2 \cdot \text{s}^{-1}]$	0.61	0.16	0.05

In other words, the energy content of 0.33 kg of hydrogen corresponds to the energy content of 1 kg of oil. The energy content of a fuel is usually called the **heating value**. The difference between the upper and the lower heating value is the enthalpy of vaporization of water (40.6 kJ/molH₂O) according to the state of the water as a result of the combustion. For hydrogen the lower heating value is 33.3 kWh·kg⁻¹, and the upper heating value is 39.4 kWh·kg⁻¹. Hydrogen is the most abundant of all elements in the universe, and it is thought that the heavy elements were, and still are, being built from hydrogen and helium. It has been estimated that hydrogen makes up for more than 90% of all the atoms or 75% of the mass of the universe [5].

There are several major technical and an economic challenges to overcome before a hydrogen energy economy becomes reality.

The **technical challenge** is the real time production, the safe and convenient storage and the efficient combustion of hydrogen.

In order to replace the world present demand of fossil fuels by hydrogen, more than 3×10^{12} kg hydrogen need to be produced per year. This is roughly 100 times today's hydrogen production. One question that can be asked is whether or not such a quantity of hydrogen could in principle be provided in a sustainable way, for example by solar energy. The solar constant is 1.362 kWm⁻² and approximately 50% of the solar radiation reaches the surface of the Earth. Standard photovoltaic systems (see for example the Appendix to Chapter IX) have an efficiency of approximately 10%, which, by the way, is the same as for biological systems based on photosynthesis (corn is one of the plants with a photoconversion efficiency of about 10%). In the best case half of the time is day and therefore, under ideal conditions about 541000 km² (90 m²/person) covered with photovoltaic cells are necessary to produce the world energy consumption (1.4×10^{14} kWh/year). This is a square with a side length of 740 km (see Fig. IX.4).

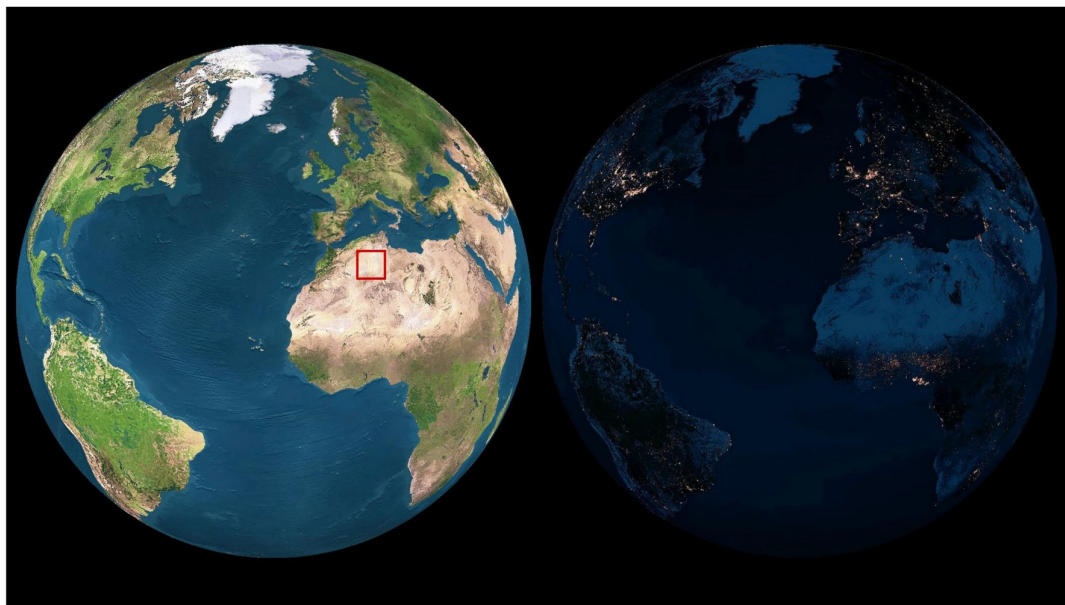


Fig. IX.4: Earth view with a square in the Sahara corresponding to the area covered with photovoltaic cells that is necessary to produce the present world energy consumption of 1.4×10^{14} kWh/year. On the right hand side Earth view during the night showing the illuminated regions were most energy is consumed.

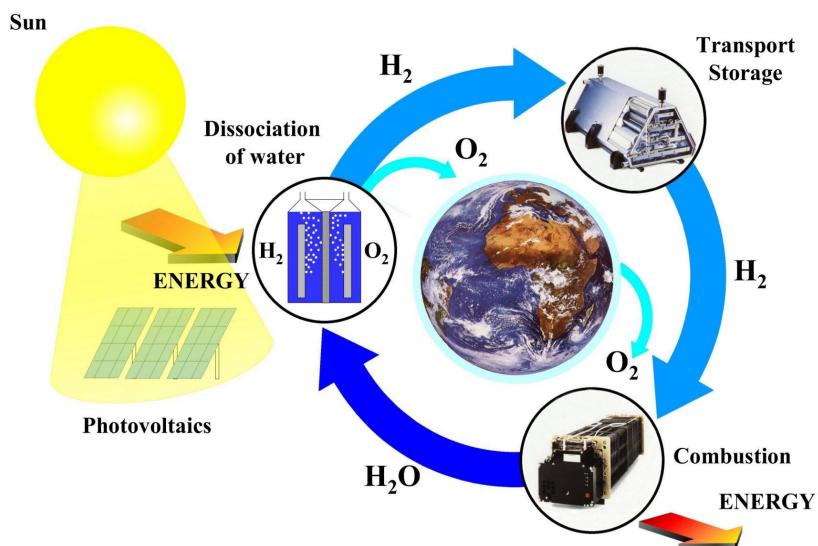


Fig. IX.5: The hydrogen cycle: Energy from sunlight is converted into electricity by means of photovoltaic cells. The electricity is used in an electrolyser (see Appendix IX.2) to dissociate water into hydrogen and oxygen. The latter is released into the atmosphere and hydrogen is stored, transported and distributed. Finally, hydrogen together with oxygen is combusted in a fuel cell (see Appendix IX.3) and the energy released as work and heat leaving water or steam into the atmosphere. Therewith the hydrogen cycle is closed.

The **economic challenge** is the cost of hydrogen production. World economy today is based on free energy naturally stored over millions of years. The price we are used to pay for fossil fuels is the mining cost only. Implementation of a synthetic fuel such as hydrogen is only possible if the world economy accepts to pay for the energy content of the fuel too. Renewable energy production requires in general investments with approximately 5 years payback. This means a worldwide investment of approximately 10^{13} to 10^{14} € ($1\text{€} \approx 1\text{ US\$}$) or in words 10 to 100 trillion Euro, i.e. the same amount as is spent worldwide for renewable energy within 5 years. The investment corresponds to approximately 20% of the annual income of a person who lives in a highly industrialized country.

Today's worldwide consumption of hydrogen as a chemical raw material (about 5×10^{10} kg/year) is produced to a large extent using fossil fuels by means of the reaction



at elevated temperature ($>850^\circ\text{C}$). This reaction is endothermic and therefore, consumes energy 8.9 kWh/kgH_2 . However, hydrogen production from fossil fuels is not renewable and produces at least the same amount of carbon dioxide as the direct combustion of the fossil fuel itself.

Hydrogen is only a renewable fuel if it is produced directly from solar light or indirectly via electricity from a renewable source e.g. wind power or hydropower.

Some of the earliest work in solar thermochemistry was dedicated to the direct thermal dissociation of water, also known as thermolysis of water, i.e. $\text{H}_2\text{O} \rightarrow \text{H}_2 + \frac{1}{2} \text{O}_2$. The processes investigated so far used a zirconia surface, solar-heated to temperatures of or above 2500 K, and subjected to a stream of water vapor [6]. The gaseous products that result from water thermolysis need to be separated at high-temperatures to avoid recombination or ending with an explosive mixture. Among the ideas proposed for separating H_2 from the products are effusion separation, and electrolytic separation. Rapid quench by injecting a cold gas or by expansion in a nozzle, followed by a low-temperature separation, are simpler and workable, but the quench introduces a significant drop in the energy efficiency of the process. Furthermore, the very high temperatures demanded by the thermodynamics of the process pose severe material problems and can lead to significant re-radiation from the reactor, thereby lowering the absorption efficiency and, consequently, further lowering the energy efficiency. These obstacles pushed the research in the direction of water-splitting thermochemical cycles.

Electricity from a renewable energy source, e.g. wind power, photovoltaics, hydropower and geothermal power can be used for the electrolysis of water. Electrolysis at ambient temperature and pressure requires a minimum voltage of 1.481V and therefore a minimum energy of 39.7 kWh/kg hydrogen. Today electrolyser systems consume approximately 47 kWh·kg⁻¹ hydrogen, i.e. the efficiency is approximately 85% [7]. (see also Appendix IX.2.3.).

Hydrogen can be transported in pipelines similarly to natural gas. There are networks for hydrogen already operating today, a 1500 km network in Europe and a 720 km network in the USA. The oldest hydrogen pipe network is in the Ruhr area in Germany and has been operated for more than 50 years. The tubes with a typical diameter of 25-30 cm are made of conventional pipe steel and operate at a pressure of 10 to 20 bar. The volumetric energy density of hydrogen gas is 36% of the volumetric energy density of natural gas at the same pressure. In order to transport the same amount of energy the hydrogen flux has to be 2.8 times larger than the flux of natural gas. However, the viscosity of hydrogen (8.92×10^{-6} Pa s) is significantly smaller than that of natural gas (11.2×10^{-6} Pa s). The minimum power P required to pump a gas through a pipe is given by

$$P = 8 \cdot \pi \cdot l \cdot v^2 \cdot \eta \quad (\text{IX.2})$$

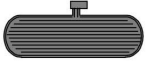
where l is the length of the pipe, v the velocity and η the dynamic viscosity of the gas. The transmission power per energy unit is therefore 2.2 times larger for hydrogen as compared to natural gas. The total energy loss during the transportation of hydrogen is about 4% of the energy content. Because of the great length, and therefore the great volume of piping systems, a slight change in the operating pressure of a pipeline system results in a large change of the amount of hydrogen gas contained within the piping network. Therefore, the pipeline can be used to handle fluctuations in supply and demand, avoiding the cost of onsite storage.

IX.2 HYDROGEN STORAGE

Hydrogen storage basically implies the reduction of the enormous volume of the hydrogen gas. One kg of hydrogen at ambient temperature and atmospheric pressure occupies a volume of 11 m³.

In order to increase the hydrogen density in a storage system, either work must be performed to compress hydrogen, or temperature has to be decreased below the critical temperature or finally, the repulsion between hydrogen molecules (or atoms) has to be reduced through interaction of hydrogen with an other material. The second important criteria for a hydrogen storage system is the reversibility of the hydrogen uptake and release. This criteria excludes all covalent hydrogen carbon compounds as hydrogen storage materials because hydrogen is only released from hydrocarbons if they are heated to temperatures above 800°C or if the carbon is oxidized. There are basically six methods in order to reversibly store hydrogen with a high volumetric and gravimetric density (see Table IX.2). The following Sections focus on these methods and illustrates there advantages and disadvantages.

Table IX.2: The six basic hydrogen storage methods and phenomena. The gravimetric density ρ_m , the volumetric density ρ_v , the working temperature T and pressure p are listed. RT stands for room temperature (25°C). From top to bottom: compressed gas (molecular H_2) in light weight composit cylinder (tensile strength of the material is 2000 MPa); liquid hydrogen (molecular H_2), continuous loss of a few % per day of hydrogen at RT; physisorption (molecular H_2) on materials e.g. carbon with a very large specific surface area, fully reversible; hydrogen (atomic H) intercalation in host metals, metallic hydrides working at RT are fully reversible; complex compounds ($[AlH_4]^-$ or $[BH_4]^-$), desorption at elevated temperature, adsorption at high pressures; chemical oxidation of metals with water and liberation of hydrogen, not directly reversible?

Storage Media	Volume	Mass	Pressure	Temperature	
	max. 33 kg $H_2 \cdot m^{-3}$	13 mass%	800 bar	298 K	Composite cylind. <i>established</i>
	71 kg $H_2 \cdot m^{-3}$	100 mass%	1 bar	21 K	Liquid hydrogen
	max. 150 kg $H_2 \cdot m^{-3}$	2 mass%	1 bar	298 K	Metalhydrides
	20 kg $H_2 \cdot m^{-3}$	4 mass%	70 bar	65 K	Physisorption
	150 kg $H_2 \cdot m^{-3}$	18 mass%	1 bar	298 K	Complex hydrides <i>reversibility ?</i>
	>100 kg $H_2 \cdot m^{-3}$	14 mass%	1 bar	298 K	Alkali + H_2O

IX.2.1 HIGH PRESSURE GAS CYLINDERS

The most common storage system uses high pressure gas cylinders with a maximum pressure of 20 MPa. New light-weight composite cylinders have been developed which are able to withstand a pressure up to 80 MPa and so the hydrogen can reach a volumetric density of $36 \text{ kg}\cdot\text{m}^{-3}$, approximately half as much as in its liquid form at the normal boiling point (see Fig.II.18). The gravimetric hydrogen density decreases with increasing pressure due to the increasing thickness of the walls of the pressure cylinder. The wall thickness of a cylinder capped with two hemispheres is given by the following equation:

$$\frac{d_w}{d_o} = \frac{\Delta p}{2 \cdot \sigma_v + \Delta p} \quad (\text{IX.3})$$

where d_w is the wall thickness, d_o the outer diameter of the cylinder, Δp the overpressure and σ_v the tensile strength of the material. The tensile strength of materials varies from 50 MPa for aluminum to more than 1100 MPa for high quality steel. Future, developments of new composite materials have a potential to increase the tensile strength above that of steel with a materials density which is less than half of the density of steel.

Most pressure cylinders today have use austenitic stainless steel (e.g. AISI 316 and 304 and AISI 316L and 304L above 300°C to avoid carbon grain-boundary segregation), copper, or aluminum alloys which are largely immune to hydrogen effects at ambient temperatures. Many other materials are subject to embrittlement and should not be used e.g. alloy or high strength steels (ferritic, martensitic, and bainitic), titanium and its alloys and some nickel based alloys.

Fig. IX.6 shows the volumetric density of hydrogen inside the cylinder and the ratio of the wall thickness to the outer diameter of the pressure cylinder for stainless steel with a tensile strength of 460 MPa. The volumetric density of hydrogen increases with pressure and reaches a maximum above 1000 bar, depending on the tensile strength of the material. However, the gravimetric density decreases with increasing pressure and the maximum gravimetric density is found for zero overpressure! Therefore, the increase in volumetric storage density is necessarily coupled to a reduction of the gravimetric density in pressurized gas systems.

The safety of pressurized cylinders is an issue of concern especially in highly populated regions. Future pressure vessels are envisaged to consist of three layers: an inner polymer liner, over-wrapped with a carbon-fiber composite (which is the stress-bearing component) and an outer layer of an aramid-material capable of withstanding mechanical and corrosion damage. The target that the industry has set for itself is a 70 MPa cylinder with a mass of 110 kg resulting in a gravimetric storage density of 6 wt% and a volumetric storage density of 30 kgm^{-3} .

Hydrogen can be compressed using standard piston-type mechanical compressors. Slight modifications of the seals are sometimes necessary in order to compensate for the higher diffusivity of hydrogen. The theoretical work necessary for the isothermal compression of one mole of hydrogen gas is approximately given by the following equation:

$$\Delta G = R \cdot T \cdot \ln\left(\frac{p_2}{p_1}\right) \quad (\text{IX.4})$$

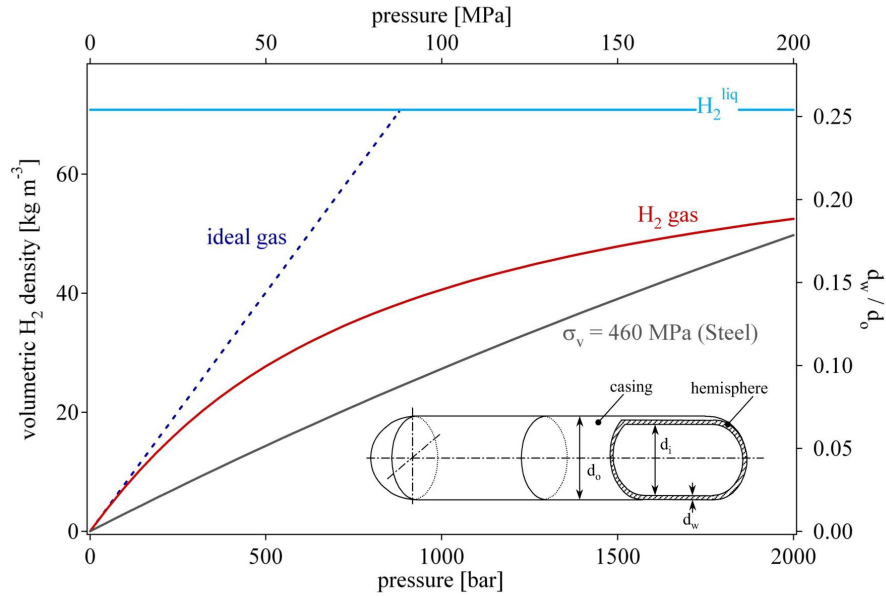


Fig. IX.6: Volumetric density of compressed hydrogen gas as a function of gas pressure including the ideal gas and liquid hydrogen. The ratio of the wall thickness to the outer diameter of the pressure cylinder is shown on the right hand side for steel with a tensile strength of 460 MPa. A schematic drawing of the pressure cylinder is shown in the inset. The deviations from the ideal gas line are a direct consequence of the non-linearity of the curves in Fig.II.17.

where p_2 and p_1 are the end pressure and the starting pressure, respectively. The error in the work calculated with equation Eq.IX.5 in the pressure range of 0.1 to 100 MPa is less than 6%. The isothermal compression of hydrogen from 0.1 MPa to 80 MPa therefore consumes 2.2 kWh/kg. In a real process the work consumption for compression is significantly higher because the compression is not isothermal. Metal-hydrides can be used to compress hydrogen from a heat source only. Compression ratios greater than 20:1 are possible with final pressures of more than 100 MPa [8].

The relatively low hydrogen density together with the very high gas pressures in the systems described here are important drawbacks of the technically simple and, on the laboratory scale, well established high pressure storage method. Nevertheless, the no-CO₂ emission busses that are scheduled to be operated in twelve European cities by the end of 2003 will use compressed hydrogen as storage system (see Fig. IX.7).



Fig. IX.7: A NEBUS (no-CO₂ emission) bus that is scheduled to be operated in twelve European cities by the end of 2003.

IX.2.2 LIQUID HYDROGEN

Liquid hydrogen is stored at ambient pressure in cryogenic tanks at 21.2 K. Due to the low critical temperature of hydrogen (33K) liquid hydrogen can only be stored in open systems, because there is no liquid phase existent above the critical temperature. The pressure in a closed storage system at room temperature could increase to about 10^4 bar. The volumetric density of liquid hydrogen is 70.8 kgm^{-3} and slightly higher than that of solid hydrogen (70.6 kgm^{-3}). The challenges of liquid hydrogen storage are the energy efficient liquefaction process and the thermal insulation of the cryogenic storage vessel in order to reduce the boil-off of hydrogen.

We show now that quantum mechanics is necessary to reduce boil-off ! As discussed in Chapter II the total wave function of the H₂ molecule has to be antisymmetric with respect to the permutation of the electrons and the protons, which are both fermions (spin = 1/2). In the ground state the electron spins are antiparallel and the spatial wave function is symmetric. The nuclear spins are also antiparallel. The total nuclear spin is then zero. The first excited state (which corresponds to a rotating molecule) has a total nuclear spin I=1 (see Fig.II.14). When the total nuclear spin I=0 the rotation quantum number J must be even (0, 2, 4,...). When I=1 the allowed values for J are 1,3, 5,... Therefore, two groups of hydrogen molecules exist according to their total nuclear spin. The first group with I = 0 is called para-hydrogen and the second group with I = 1 is called ortho-hydrogen. Normal hydrogen at room temperature contains 25% para-hydrogen and 75% ortho-hydrogen. The ortho-form cannot be prepared in the pure state. Since the two forms differ in energy, their physical properties are different. The melting and boiling points of para-hydrogen are about 0.1 K lower than those of normal hydrogen (see Table II.4). At zero Kelvin, all the molecules must be in a rotational ground state i.e. in the para-form.

When hydrogen is cooled from room temperature (RT) to the normal boiling point (nbp = 21.2K) ortho-hydrogen converts from an equilibrium concentration of 75% at RT to 50% at 77K and 0.2% at nbp. These values are equilibrium values. In fact it turns out that the self-conversion rate is a very slow activated process with a conversion half-life time longer than one year at 77K. The

conversion reaction from ortho- to para-hydrogen is exothermic and the heat of conversion is also temperature dependent. At 300K the heat of conversion is $270 \text{ kJ}\cdot\text{kg}^{-1}$ and increases as the temperature decreases, where it reaches $519 \text{ kJ}\cdot\text{kg}^{-1}$ at 77K. At temperatures lower than 77K the enthalpy of conversion is $523 \text{ kJ}\cdot\text{kg}^{-1}$ and almost constant. The enthalpy of conversion is greater than the latent heat of vaporization ($H_v = 451.9 \text{ kJ}\cdot\text{kg}^{-1}$) of normal and para-hydrogen at the nbp. This implies that when unconverted normal hydrogen is placed in a storage vessel, the enthalpy of conversion is released within the vessel, which leads to an extra evaporation of the liquid hydrogen. This can be avoided by speeding up the transformation from ortho- to para-hydrogen during liquefaction. For this one can use a number of surface active and paramagnetic species. Unconverted hydrogen can, for example, be adsorbed on charcoal cooled with liquid hydrogen and desorbed as an equilibrium mixture. The conversion may take only a few minutes if a highly active form of charcoal is used. Other suitable ortho-para catalysts are metals such as tungsten, nickel, or any paramagnetic oxides like chromium or gadolinium oxides. The nuclear spin is reversed without breaking the H-H bond.

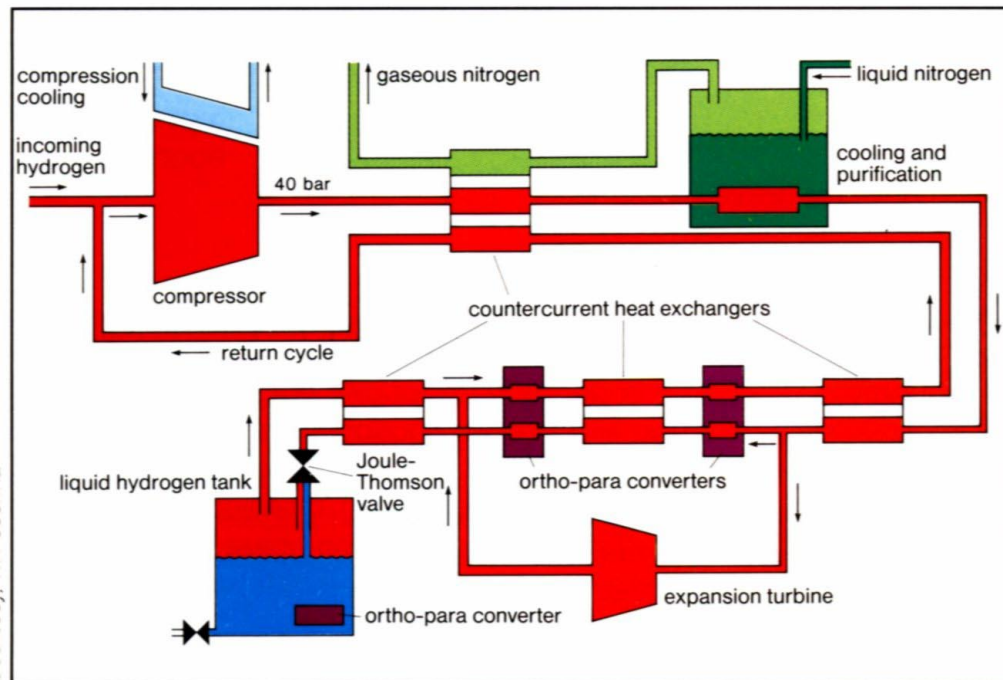


Fig. IX.8: The Joule-Thompson cycle (Linde cycle). The gas is first compressed, and then cooled in a heat exchanger, before it passes through a throttle valve where it undergoes an isenthalpic Joule-Thomson expansion, producing some liquid. The cooled gas is separated from the liquid and returned to the compressor via the heat exchanger

The simplest liquefaction cycle, the so-called Joule-Thompson cycle (Linde cycle) is shown in Fig. IX.8. The gas is first compressed, and then cooled in a heat exchanger, before it passes through a throttle valve where it undergoes an isenthalpic Joule-Thomson expansion, producing some liquid. The cooled gas is separated from the liquid and returned to the compressor via the heat exchanger [9]. The Joule-Thompson cycle works for gases, such as nitrogen, with a inversion temperature above room temperature. Hydrogen, however, warms upon expansion at room temperature. In order for hydrogen to cool upon expansion, its temperature must be below its

inversion temperature of 202K . Therefore, hydrogen is usually pre-cooled using liquid nitrogen (78K) before the first expansion step occurs. The free enthalpy change between gaseous hydrogen at 300K and liquid hydrogen at 20K is $11640 \text{ kJ}\cdot\text{kg}^{-1}$ [10]. The necessary theoretical energy (work) to liquefy hydrogen from RT is $W_{\text{th}} = 3.23 \text{ kWh}\cdot\text{kg}^{-1}$, the technical work is about $15.2 \text{ kWh}\cdot\text{kg}^{-1}$ [11] almost half of the lower heating value of the hydrogen combustion (see Table IX.1).

The boil-off rate of hydrogen from a liquid hydrogen storage vessel due to thermal leaks is a function of the size, the shape and the thermal insulation of the vessel. Theoretically the best shape is a sphere since it has the smallest surface-to-volume ratio and since stress and strain are distributed uniformly. However, large size, spherical containers are expensive because of their manufacturing difficulty. Since boil-off losses due to heat leaks are proportional to the surface-to-volume ratio, the evaporation rate diminishes drastically as the storage tank size increases. For double-walled vacuum-insulated spherical Dewars, boil-off losses are typically 0.4% per day for tanks which have a storage volume of 50 m^3 , 0.2% for 100m^3 tanks, and 0.06% for 20000m^3 tanks.



Fig. IX.9: Trailer for liquid H_2 transport (total weight 40 tons; load 3370 kg)

Low temperature para-hydrogen requires the use of materials which retain good ductility at low temperatures. Austenitic stainless steel (e.g. AISI 316L and 304L) or aluminum and aluminum alloys (Serie 5000) are recommended. Polytetrafluorethylene (PTFE, Teflon[®]) and 2-Chloro-1,1,2-trifluoroethylene (Kel-F[®]) can also be used.

The relatively large amount of energy necessary for the liquefaction and the continuous boil-off of hydrogen limit the possible applications of liquid hydrogen storage systems to niches where the cost of hydrogen is not an important issue and the hydrogen is consumed in a rather short time, e.g. air and space applications.



Fig. IX.10: BMW 745i refilled with liquid hydrogen (left photograph). Exploded view of the liquid hydrogen tank (right panel).

IX.2.3 PHYSISORPTION OF HYDROGEN

The adsorption of a gas on a surface is a consequence of the field force at the surface of the solid, called the **adsorbent**, which attracts the molecules of the gas or vapor, called **adsorbate**. The origin of the physisorption of gas molecules on the surface of a solid are resonant fluctuations of the charge distributions and are therefore called dispersive interactions or Van der Waals interactions. In the physisorption process a gas molecule interacts with several atoms at the surface of the solid. The interaction is composed of two terms: an attractive term which diminishes with the distance between the molecule and the surface r^{-6} and a repulsive term which varies as r^{-12} . Therefore, the potential energy of the molecule exhibits a minimum at a distance of approximately one molecular radius of the adsorbate. The energy minimum is of the order of 0.01 to 0.1 eV (1 to 10 $\text{kJ}\cdot\text{mol}^{-1}$) [12]. Due to the weak interaction, a significant physisorption is only observed at low temperatures ($< 273 \text{ K}$).

Once a monolayer of adsorbate molecules is formed the gaseous molecule interact with a surface of the liquid or solid adsorbate. Therefore, the binding energy of the second layer of adsorbate molecules is similar to the latent heat of sublimation or vaporization of the adsorbate. Consequently, the adsorption of the adsorbate at a temperature equal or greater to the boiling point at a given pressure leads to the adsorption of one single monolayer [13].

In order to estimate the quantity of adsorbate in the monolayer the density of the liquid adsorbate and the volume of the molecule must be used. If the liquid is assumed to consist of a closed packed fcc structure, the minimum surface area S_{ml} for one mole of adsorbate in a monolayer on a substrate can be calculated from the density of the liquid ρ_{liq} and the molecular mass of the adsorbate M_{ads} .

$$S_{ml} = \frac{\sqrt{3}}{2} \cdot \left(\sqrt{2} \cdot N_A \cdot \frac{M_{ads}}{\rho_{liq}} \right)^{\frac{2}{3}} \quad (\text{IX.5})$$

where N_A stands for the Avogadro constant ($N_A = 6.022 \cdot 10^{23} \text{ mol}^{-1}$). The monolayer surface area for hydrogen is $S_{m}(\text{H}_2) = 85917 \text{ m}^2 \text{ mol}^{-1}$. The amount of adsorbate m_{ads} on a substrate material with a specific surface area S_{spec} is then given by $m_{\text{ads}} = M_{\text{ads}} \times S_{\text{spec}} / S_{\text{ml}}$. For the adsorption of hydrogen on carbon (with a maximum specific surface area $S_{\text{spec}} = 1315 \text{ m}^2 \cdot \text{g}^{-1}$ (single side graphene sheet)) the maximum amount of adsorbed hydrogen is $m_{\text{ads}} = 3.0 \text{ wt}\%$. From this theoretical approximation we may conclude that the amount of adsorbed hydrogen is proportional to the specific surface area of the adsorbent with $m_{\text{ads}}/S_{\text{spec}} = 2.27 \cdot 10^{-3} \text{ wt}\% \cdot \text{m}^{-2} \text{ g}$ and can only be observed at very low temperatures.

Much work on reversible hydrogen sorption of carbon nanostructures was stimulated by the work of Dillon et al. [14]. This paper describes the results of a brief hydrogen desorption experiment. The authors estimated the hydrogen storage capacity of carbon nanotubes at that time to be 5 to 10 wt%. The investigation was carried out on a carbon sample containing an estimated (TEM micrographs) amount of 0.1 to 0.2 wt% of single wall carbon nanotubes (SWNT). The amount of hydrogen desorbed in the high-temperature peak, which is roughly 5 to 10 times smaller than the low temperature physisorption peak, was 0.01 wt%. The authors concluded “Thus the gravimetric storage density per SWNT ranges from 5 to 10 wt%”. Three years later in a report to the American Department of Energy (DOE) [15] this peak has moved significantly by 300 K up to 600 K. Apparently the reported results are inconsistent. Hirscher et al. [16] clarified the situation and showed that the desorption of hydrogen originates from Ti-alloy particles in the sample, introduced during the ultrasonic pre-treatment, rather than from the carbon nanotubes.

The main difference between carbon nanotubes and high surface area graphite is the curvature of the graphene sheets and the cavity inside the tube. In microporous solids with capillaries which have a width not exceeding a few molecular diameters, the potential fields from opposite walls will overlap so that the attractive force which acts upon adsorbate molecules is larger than that on a flat carbon surface [17]. This phenomenon is the main motivation for the investigation of the hydrogen interaction with carbon nanotubes.

Most papers reporting theoretical studies on hydrogen absorption in carbon nanostructures focus on the physisorption of H_2 on carbon using the grand canonical Monte Carlo simulation. Stan and Cole [18] used the Feynman (semiclassical) effective potential approximation to calculate the adsorption potential and the amount of hydrogen adsorbed on a zigzag nanotube (13,0) with a diameter of 1.018 nm. The adsorption potential was found to be 9 kJ mol^{-1} (0.093 eV) for hydrogen molecules inside the nanotubes at 50 K, the potential is about 25% higher than that of a flat surface of graphite due to the curvature of the surface. Therefore an increased number of carbon atoms interacts with the hydrogen molecule. The ratio of hydrogen adsorbed in the tube to that on a flat surface decreases strongly with increasing temperature and is 10000 at 50 K and 100 at 77 K. Rzepka et al. [19] used a grand canonical ensemble Monte Carlo program to calculate the amount of adsorbed hydrogen for a slit pore and a tubular geometry. The amount of adsorbed hydrogen depends on the surface area of the sample, the maximum is at 0.6 wt% ($p = 6 \text{ MPa}$, $T = 300 \text{ K}$). The calculation was experimentally verified with excellent agreement. At a temperature of 77 K the amount of adsorbed hydrogen is about one order of magnitude higher compared to 300 K. Williams and Eklund [20] performed grand canonical Monte Carlo simulation of H_2 physisorption in finite-diameter carbon SWNT ropes and found an increasing amount of adsorbed hydrogen with decreasing temperature from 1.4 wt% ($p = 10 \text{ MPa}$, $T = 300 \text{ K}$) to 9.6 wt% ($p = 10 \text{ MPa}$, $T = 77 \text{ K}$). For lower hydrogen pressure this range is shifted to considerably lower amounts of adsorbed hydrogen, i.e. 0.2 wt% ($p = 1 \text{ MPa}$, $T = 300 \text{ K}$) to 5.9 wt% ($p = 10 \text{ MPa}$, $T = 77 \text{ K}$). Lee et al. [21] have performed density-functional and density-functional-based tight-binding calculations to search for hydrogen chemisorption sites on single wall-nanotubes. The

investigation of the absorption of hydrogen inside the tubes has shown that it is energetically more favorable for the hydrogen atoms to recombine and form molecules, which are then physisorbed inside the nanotube. Ma et al. [22] performed a molecular dynamics simulation for H implantation. Hydrogen atoms were implanted at 20 eV through the sidewalls of a single wall carbon nanotube (5,5) consisting of 150 atoms and have a diameter of 0.683 nm. They found that the hydrogen atoms recombine to molecules inside the tube and arrange themselves to a concentric tube. The hydrogen pressure inside the SWNT increases as the number of injected atoms increases and reaches 35 GPa for 90 atoms (5 wt%). This simulation does not exhibit a condensation of hydrogen inside the nanotube. The critical temperature of hydrogen (H_2) is 33.25K [23]. Therefore, at temperatures above 33.25 K and at all pressures, hydrogen does not exist as a liquid phase, hydrogen is either a gas or a solid. The density of liquid and solid hydrogen at the melting point ($T_m = 14.1$ K) is 70.8 kg m^{-3} and 70.6 kg m^{-3} , respectively. The measurement of the latent heat of condensation of nitrogen on carbon black [24] showed, that the heat for the adsorption of one monolayer is between 11 to $12 \text{ kJ}\cdot\text{mol}^{-1}$ (0.11 to 0.12 eV) and drops for subsequent layers to the latent heat of condensation for nitrogen which is 5.56 kJ mol^{-1} (0.058eV). If we assume, that hydrogen behaves in a similar manner to nitrogen, then hydrogen would only form one monolayer of liquid at the surface of carbon at temperatures above the boiling point. Geometrical considerations of the nanotubes lead to the specific surface area and therefore, to the maximum amount of condensed hydrogen in a surface monolayer. Fig. IX.11 shows the maximum amount of hydrogen in wt% for the physisorption of hydrogen on carbon nanotubes [25]. The maximum amount of adsorbed hydrogen is 2.0 wt% for single wall carbon nanotubes (SWNT) with a specific surface area of $1315 \text{ m}^2 \text{ g}^{-1}$ at a temperature of 77K.

Experiments on hydrogen absorption in carbon nanostructures were carried out with different methods under various conditions and on plenty of small and often not very well characterized samples. Hydrogen gas adsorption isotherms ($T = 80$ K) were performed by Ye et al. on purified SWNT samples [26]. The BET surface area of the SWNT sample was found to be $285 \text{ m}^2\text{g}^{-1}$ and remained unchanged upon the hydrogen absorption and desorption. The hydrogen adsorption obtained at a temperature of 80K and a pressure of 0.32 MPa was $H/C = 0.04$ for the SWNT sample and was $H/C = 0.28$ for the high surface area saran-carbon ($1600 \text{ m}^2\text{g}^{-1}$). At high hydrogen pressures (7 MPa) at a temperature of 80 K, the hydrogen to carbon ratio for the SWNT sample reached $H/C = 1$ (7.7 mass%) in the initial absorption. In the following absorption cycles the absorption isotherm shifted considerably to higher pressure. The hydrogen to carbon ratio of $H/C = 0.8$ was reached at 12 MPa. Liu et al. [27] applied high pressure (12 MPa) hydrogen gas at room temperature (298 K) to SWNT and followed the pressure change with time. The samples equilibrated after approximately 300 minutes and reached a maximum absorption of 4.2 mass% ($H/C = 0.5$). About 20% of the absorbed hydrogen remained in the sample after desorption at room temperature. Fan et al. [28] investigated the hydrogen absorption of vapor-grown carbon nanofibers with a diameter of 5 nm to 300 nm. The fibers absorbed hydrogen up to 12.38 mass% when a hydrogen pressure of 12 MPa was applied. The absorption equilibrated after 200 - 300 minutes. Chen et al [29] reported that a high hydrogen uptake of 14 mass% to 20 mass% can be achieved for K- and Li-doped MWNT, respectively, at a pressure of 0.1 MPa. The K-doped MWNT absorb hydrogen at room temperature, but they are chemically unstable, whereas the Li-doped MWNT are chemically stable, but require elevated temperatures (473 - 673 K) for maximum absorption and desorption of hydrogen. However, the increase of the mass observed upon hydrogen absorption was due to impurities like oxygen and water and therefore due to the oxidation of the alkali metals [30] rather than a hydrogen uptake.

A large variety of carbon samples was investigated by Ströbel et al. [31], using a high-pressure microbalance. The BET (N_2) surface area of the samples ranges from $100 \text{ m}^2\text{g}^{-1}$ up to $3300 \text{ m}^2\text{g}^{-1}$. The absorbed amount of hydrogen ($p = 12.5 \text{ MPa}$, $T = 296 \text{ K}$) correlates with the surface area according to the equation $x \text{ [mass\%]} = 0.0005 \cdot S[\text{m}^2\text{g}^{-1}]$ (taken from figure) except for the nano fiber samples. The latter exhibit a rather low surface area of approximately $100 \text{ m}^2\text{g}^{-1}$; however, the increase in mass upon hydrogen absorption corresponds to about 1.2 mass%. The measured adsorption isotherms approximately follow the Langmuir adsorption model. Some isotherms intercept the mass-axis ($p = 0$) at $x = 0$, other intercept at a finite mass between 0.2 and 0.4 mass%. Nijkamp et al. [32] characterised a large number of carbonaceous sorbents using N_2 physisorption at 77 K and up to a pressure of 1 bar. The sorbents were chosen to represent a large variation in surface areas and (micropores) volumes. Both non-porous materials, such as aerosil and graphites, and microporous sorbents, such as activated carbons and zeolites, were selected.

The H_2 -adsorption measurements were performed at 77 K in the pressure range 0–1 bar. From adsorption–desorption experiments it is evident that exclusively reversible physisorption takes place in all samples. The amount of adsorbed hydrogen correlates with the specific surface area of the sample (Fig. IX.11). A few papers on electrochemical measurements at room temperature of hydrogen uptake and release have been published [33–36]. The electrochemical hydrogen absorption is reversible. The maximum discharge capacity measured at 298 K is 2 mass% with a very small discharge current (discharge process for 1000h).

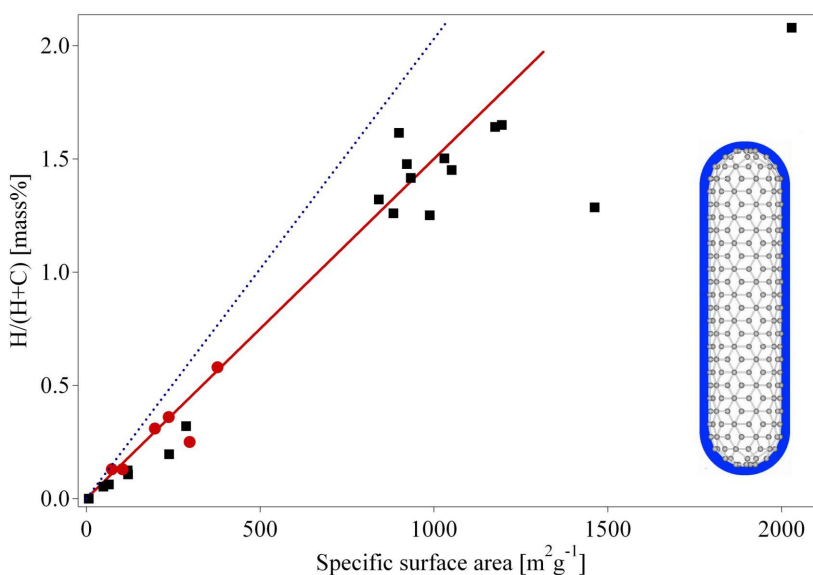


Fig. IX.11: Reversible amount of hydrogen (electrochemical measurement at 298 K) versus the B.E.T. surface area (round markers) of a few carbon nanotube samples including two measurements on high surface area graphite (HSAG) samples together with the fitted line. Hydrogen gas adsorption measurements at 77 K from Nijkamp et al. [32] (square markers) are included. The dotted line represents the calculated amount of hydrogen in a monolayer at the surface of the substrate.

It is remarkable, that the measurements of the hydrogen uptake in the gas phase at 77 K exhibit the same quantities as the electrochemical measurements at room temperature 298 K. In the electrochemical charging process hydrogen atoms are left back at the surface of the electrode when the electron transfer from the conductor to the water molecules takes place. The hydrogen atoms recombine to hydrogen molecules. This process goes on until the surface is completely covered with a monolayer of physisorbed H₂ molecules. Additional hydrogen does not interact with the attractive Van der Waals forces of the surface. The hydrogen molecules become very mobile and form gas bubbles, which are released from the electrode surface. The formation of a stable monolayer of hydrogen at the electrode surface at room temperature is only possible if either the hydrogen atoms or the hydrogen molecules are immobile, i.e. their surface diffusion has to be kinetically hindered by a large energy barrier probably due to the adsorbed electrolyte (H₂O) molecules in the second layer. An other possible reaction path was first reported [21] as a result of density-functional calculation. The result of this calculation is that hydrogen atoms tend to chemisorb at the exterior surface of a nanotube. The atoms can then flip in and recombine to hydrogen molecules finally at high coverage forming a concentric cylinder in the cavity of the nanotube. If the binding energy of the chemisorbed hydrogen is relatively low compared to the energy in hydrocarbons, the absorbed amount of hydrogen is proportional to the surface area of the carbon sample and could also desorb at rather positive electrochemical potential.

In conclusion: the reversible hydrogen sorption process is based on the physisorption. The amount of adsorbed hydrogen is proportional to the BET surface area of the nanostructured carbon sample. The amount of adsorbed hydrogen from the gas phase at 77 K and electrochemically at room temperature is $1.5 \cdot 10^{-3} \text{ mass}\% \cdot \text{m}^{-2} \text{ g}$. Together with the maximum specific surface area of carbon ($1315 \text{ m}^2 \text{ g}^{-1}$) the maximum absorption capacity of carbon nanostructures is 2 mass%. The experimental results are in good agreement with the theoretical estimations if we take into account that the measurements were carried out at a temperature of 77 K which is still far above the critical temperature of hydrogen of 32 K and therefore the monolayer of hydrogen is not complete at 77K. No evidence of an influence of the geometric structure of the nanostructured carbon on the amount of adsorbed hydrogen was found. It's quite obvious, that the curvature of nanotubes may only influence the adsorption energy but not the amount of adsorbed hydrogen. Furthermore, all attempts to open the nanotubes and to absorb hydrogen inside the tubes did not show an increased absorption of hydrogen molecules. Theoretical studies beyond the well-known physisorption lead to a large set of various maximum hydrogen absorption capacities. Most of the results were found under special conditions, e.g. at 0 K or high energy hydrogen atom implantation. No evidence was found for a higher density of hydrogen in and on carbon nanostructures compared to liquid hydrogen at ambient conditions.

Beside the carbon nanostructures, other nanoporous materials have been investigated for hydrogen absorption. The hydrogen absorption of zeolites of different pore architecture and composition, e.g. A, X, Y, was analyzed in the temperature range from 293K to 573K and pressure range from 2.5 MPa to 10 MPa [37]. Hydrogen was absorbed at the desired temperature and pressure. The sample was then cooled to room temperature and evacuated. Subsequently the hydrogen release upon heating of the sample to the absorption temperature was detected. The absorbed amount of hydrogen increased with increasing temperature and increasing absorption pressure. The maximum amount of desorbed hydrogen was found to be 0.08 mass% for a sample loaded at a temperature of 573K and a pressure of 10 MPa [37]. The adsorption behavior indicates that the absorption is due to a chemical reaction rather than physisorption. At liquid nitrogen

temperature (77 K) the zeolites physisorb hydrogen proportional to the specific surface area of the material. A maximum of 1.8 mass% of adsorbed hydrogen was found for a zeolite (NaY) with a specific surface area of $725 \text{ m}^2 \cdot \text{g}^{-1}$ [38]. The low temperature physisorption (type I isotherm) of hydrogen in zeolites is in good agreement with the adsorption model mentioned above for nanostructured carbon. The desorption isotherm followed the same path as the adsorption [38] which indicates that no pore condensation occurred. Recently a microporous metal-organic framework of the composition $\text{Zn}_4\text{O}(\text{1,4-benzenedicarboxylate})_3$ was proposed as hydrogen storage material [39]. The material absorbs hydrogen at a temperature of 298 K proportional to the applied pressure. The slope of the linear relationship between the gravimetric hydrogen density and the hydrogen pressure was found to be $0.05 \text{ mass}\% \cdot \text{bar}^{-1}$. No saturation of the hydrogen absorption was found, which is very unlikely for any kind of a hydrogen absorption process. At 77 K the amount of adsorbed hydrogen was detected to be 3.7 mass% already at very low hydrogen pressure and a slight almost linear increase with increasing pressure. This behavior is not a type I isotherm as the authors claimed and the results should be taken with care.

The big advantages of the physisorption for hydrogen storage are the low operating pressure, the relatively low cost of the materials involved and the simple design of the storage system. The rather small amount of adsorbed hydrogen on carbon together with the low temperatures necessary are significant drawbacks of the hydrogen storage based on physisorption.

IX.2.4 METALHYDRIDES

Metals, intermetallic compounds and alloys generally react with hydrogen and form mainly solid metal-hydrogen compounds. Hydrides exist as ionic, polymeric covalent, volatile covalent and metallic hydrides. The demarcation between the various types of hydrides is not sharp, they merge into each other according to the electronegativities of the elements concerned. This Section focuses on metallic hydrides, i.e. metals and intermetallic compounds which form together with hydrogen metallic hydrides. Hydrogen reacts at elevated temperature with many transition metals and their alloys to form hydrides. The electropositive elements are the most reactive, i.e., scandium, yttrium, the lanthanides, the actinides, and the members of the titanium and vanadium groups. The binary hydrides of the transition metals are predominantly metallic in character and are usually referred to as metallic hydrides. They are good conductors of electricity, possess a metallic or graphite.

Many aspects of metal-hydrides are dealt with in the other Chapters of these lecture notes. Here we focus on the aspects that are of direct relevance to hydrogen storage.

Many of these compounds (MH_n) show large deviations from ideal stoichiometry ($n = 1, 2, 3$) and can exist as multi-phase systems. The lattice structure is that of a typical metal with atoms of hydrogen on the interstitial sites; for this reason they are also called interstitial hydrides. This type

Allred-Rochow Electronegativity Ref: Huheey, J.E. Inorganic Chemistry ; Harper & Row: New York, 1983

1		2										13						14	15	16	17	18	
H																						He	
2.20																							
LiH		BeH ₂																BH ₃	CH ₄	NH ₃	H ₂ O	HF	Ne
0.97		1.47																2.01	2.50	3.07	3.50	4.10	
NaH		MgH ₂																AlH ₃	SiH ₄	PH ₃	H ₂ S	HCl	Ar
1.01		1.23																1.47	1.74	2.06	2.44	2.83	
KH		CaH ₂	ScH ₂	TiH ₂	VH	VH ₂	CrH	CrH ₂	Mn	Fe	Co	NiH _{<1}	CuH	ZnH ₂	(GaH ₃)	GeH ₄	AsH ₃	H ₂ Se	HBr	Kr			
0.91		1.04	1.20	1.32	1.45	1.56	1.60	1.64	1.70	1.75	1.75	1.75	1.66	1.82	2.02	2.20	2.48	2.74					
RbH		SrH ₂	YH ₂	YH ₃	ZrH ₂	(NbH ₂)	Mo	Tc	Ru	Rh	PdH _{<1}	Ag	(CdH ₂)	(InH ₃)	SnH ₄	SbH ₃	H ₂ Tc	HI	Xe				
0.89		0.99	1.11	1.22	1.23	1.30	1.36	1.42	1.45	1.45	1.35	1.42	1.46	1.49	1.72	1.82	2.01	2.21					
CsH		BaH ₂	LaH ₂	LaH ₃	HfH ₂	Ta	W	Re	Os	Ir	Pt	(AuH ₃)	(HgH ₂)	(TlH ₃)	PbH ₄	BiH ₃	H ₂ Po	HAt	Rn				
0.86		0.97	1.08	1.23	1.33	1.40	1.46	1.52	1.55	1.44	1.42	1.44	1.44	1.44	1.55	1.67	1.76	1.90					
Fr		Ra	AcH ₂																				
			1.00																				

CeH ₃	PrH ₂	PrH ₃	NdH ₂	NdH ₃	Pm	SmH ₂	SmH ₃	EuH ₂	GdH ₂	GdH ₃	TbH ₂	TbH ₃	DyH ₂	DyH ₃	HoH ₂	HoH ₃	ErH ₂	ErH ₃	TmH ₂	TmH ₃	(YbH ₂)	(YbH ₃)	LuH ₂	LuH ₃
1.06	1.07	1.07	1.07			1.07	1.01	1.11	1.11	1.11	1.10	1.10	1.10	1.10	1.10	1.11	1.11	1.11	1.11	1.11	1.06	1.14		
ThH ₂	PaH ₂	UH ₃	NpH ₂	NpH ₃	PuH ₂	PuH ₃	AmH ₂	AmH ₃	Cm	Bk	Cf	Es	Fm	Md	No	Lr								
1.11	1.14	1.22	1.22	1.22	1.22	1.2																		

Table IX.3 Table of the binary hydrides and the Allred-Rochow electronegativity Ref.: Huheey, J.E. Inorganic Chemistry ; Harper & Row: New York, 1983. Most elements react with hydrogen to form ionic, covalent or metallic binary hydrides. -like appearance, and can often be wetted by mercury.

of structure has the limiting compositions MH, MH₂, and MH₃; the hydrogen atoms fit into octahedral or tetrahedral holes in the metal lattice, or a combination of the two types. The hydrogen carries a partial negative charge, depending on the metal an exception is, for example, PdH_{0.7} [40]. Only a small number of the transition metals are without known stable hydrides. A considerable "hydride gap" exists in the periodic table, beginning at group 6 (Cr) up to group 11 (Cu), in which the only hydrides are palladium hydride (PdH_{0.7}), the very unstable nickel hydride (NiH_{<1}), and the poorly defined hydrides of chromium (CrH, CrH₂) and copper (CuH). In palladium hydride, the hydrogen has high mobility and probably a very low charge density. In the finely divided state, platinum and ruthenium are able to adsorb considerable quantities of hydrogen, which thereby becomes activated. These two elements, together with palladium and nickel, are extremely good hydrogenation catalysts, although they do not form hydrides [41]. Especially interesting are the metallic hydrides of intermetallic compounds, in the simplest case the ternary system AB_xH_n, because the variation of the elements allows to tailor the properties of the hydrides (Table IX.4).

Table IX.4: The most important families of hydride forming intermetallic compounds including the prototype and the structure. A is an element with a high affinity to hydrogen, and B is an element with a low affinity to hydrogen.

Intermetallic compound	Prototype	Hydrides	Structure
AB ₅	LaNi ₅	LaNiH ₆	Haucke phases, hexagonal
AB ₂	ZrV ₂ , ZrMn ₂ , TiMn ₂	ZrV ₂ H _{5.5}	Laves phase, hexagonal or cubic
AB ₃	CeNi ₃ , YFe ₃	CeNi ₃ H ₄	hexagonal, PuNi ₃ -typ
A ₂ B ₇	Y ₂ Ni ₇ , Th ₂ Fe ₇	Y ₂ Ni ₇ H ₃	hexagonal, Ce ₂ Ni ₇ -typ
A ₆ B ₂₃	Y ₆ Fe ₂₃	Ho ₆ Fe ₂₃ H ₁₂	cubic, Th ₆ Mn ₂₃ -typ
AB	TiFe, ZrNi	TiFeH ₂	cubic, CsCl- or CrB-typ
A ₂ B	Mg ₂ Ni, Ti ₂ Ni	Mg ₂ NiH ₄	cubic, MoSi ₂ - or Ti ₂ Ni-typ

The A element is usually a Rare Earth or an Alkaline Earth metal and tends to form a stable hydride. The B element is often a transition metal and forms only unstable hydrides. Some well defined ratios of B to A in the intermetallic compound $x = 0.5, 1, 2, 5$ have been found to form hydrides with a hydrogen-to-metal ratio of up to two.

The reaction of hydrogen gas with a metal is called the absorption process and can be described in terms of a simplified one-dimensional potential energy curve (one-dimensional Lennard-Jones potential, Fig. IX.12) [42].

Far from the metal surface the potential of a hydrogen molecule and of 2 hydrogen atoms are separated by the dissociation energy ($H_2 \rightarrow 2H$, $E_D = 435.99 \text{ kJ}\cdot\text{mol}/H_2$). The first attractive interaction of the hydrogen molecule approaching the metal surface is the Van der Waals force leading to the physisorbed state ($E_{\text{phys}} \approx -5 \text{ kJ}/\text{molH}$) approximately one hydrogen molecule radius ($\approx 0.2 \text{ nm}$) from the metal surface. Closer to the surface hydrogen has to overcome an activation barrier for dissociation and formation of the hydrogen metal bond. The height of the activation barrier depends on the surface elements involved. Hydrogen atoms sharing their electron with the metal atoms at the surface are then in the chemisorbed state ($E_{\text{chem}} \approx -60 \text{ kJ}/\text{molH}$). The chemisorbed hydrogen atoms may have a high surface mobility, interact with each other and form surface phases at sufficiently high coverage. In the next step the chemisorbed hydrogen atom can jump in the subsurface layer and finally diffuse on the interstitial sites through the host metal lattice. The hydrogen atoms contribute with their electron to the band structure of the metal.

The hydrogen is at small hydrogen to metal ratio ($H/M < 0.1$) exothermically dissolved (solid-solution, α -phase) in the metal. The metal lattice expands proportionally to the hydrogen concentration by approximately 2 to 3\AA^3 per hydrogen atom [43]. At greater hydrogen concentrations in the host metal ($H/M > 0.1$) a strong H-H interaction due to the lattice expansion (see Chapter IV.6) becomes important and the hydride phase (β -phase) nucleates and grows. The hydrogen concentration in the hydride phase is often found to be $H/M = 1$. The volume expansion between the coexisting α - and the β -phase corresponds in many cases to 10 to 20% of the metal lattice. Therefore, at the phase boundary large stresses are built up and often leads to a decrepitation of brittle host metals such as intermetallic compounds. The final hydride is a powder with a typical particle size of 10 to 100 μm .

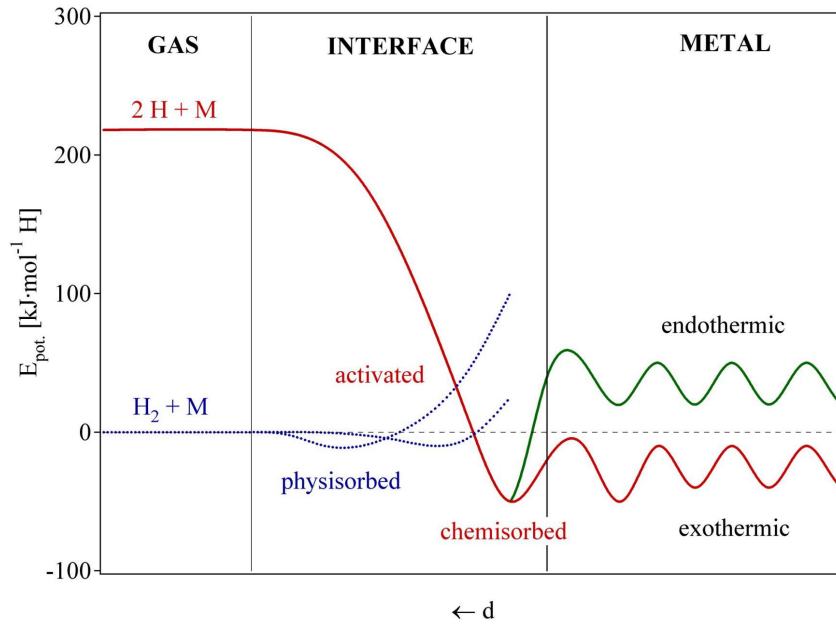


Fig. IX.12: Lennard-Jones potential of hydrogen approaching a metallic surface. Far from the metal surface the potential of a hydrogen molecule and of 2 hydrogen atoms are separated by the dissociation energy. The first attractive interaction of the hydrogen molecule is the Van der Waals force leading to the physisorbed state. Closer to the surface hydrogen has to overcome an activation barrier for dissociation and formation of the hydrogen metal bond. Hydrogen atoms sharing their electron with the metal atoms at the surface are then in the chemisorbed state. In the next step the chemisorbed hydrogen atom can jump in the subsurface layer and finally diffuse on the interstitial sites through the host metal lattice.

The thermodynamic aspects of the hydride formation from gaseous hydrogen is described by means of pressure-composition isotherms (see Fig. IX.13 and Chapter III). When the solid solution and hydride phase coexist, the isotherms show a flat plateau, the length of which determines the amount of H_2 stored. In the pure β -phase, the H_2 pressure rises steeply with the concentration. The two-phase region of the phase diagram ends at the critical point T_C , above which the transition from α - to β -phase is continuous (see Chapter IV). The equilibrium pressure p as a function of temperature is related to the changes ΔH and ΔS of enthalpy and entropy, respectively, by the Van't Hoff equation (see Eq.III.102) :

$$\frac{1}{2} \ln p = \frac{\Delta H_{\alpha \rightarrow \beta}}{RT} - \frac{\Delta S_{H_2}}{2R} = \frac{\Delta H_{\alpha \rightarrow \beta}}{RT} + \frac{S_{H_2}^0}{2R} \quad (\text{IX.6})$$

As the entropy change corresponds mostly to the change from molecular hydrogen gas to dissolved solid hydrogen, it amounts approximately to the standard entropy of hydrogen ($S_{H_2}^0 = 130.8 \text{ J/K/molH}_2$) and is therefore, essentially the same for all metal-hydrogen systems. The enthalpy term characterizes the stability of the metal-hydrogen bond. To reach an equilibrium pressure of 1 bar at 300K ΔH should amount to approximately -20 kJ/molH. The entropy of

formation term of metal hydrides leads to a significant heat evolution $\Delta Q = T \cdot \Delta S$ (exothermal reaction) during the hydrogen absorption. The same heat has to be provided to the metal-hydride to desorb the hydrogen (endothermal reaction). If the hydrogen desorbs below room temperature this heat can be delivered by the environment. However, if the desorption is carried out above room temperature the necessary heat has to be delivered at the necessary temperature by an external source, which may be the combustion of the hydrogen itself. For a stable hydride such as MgH_2 the heat necessary for the desorption of hydrogen at 300°C and 1 bar is approximately 25% of the higher heating value of hydrogen.

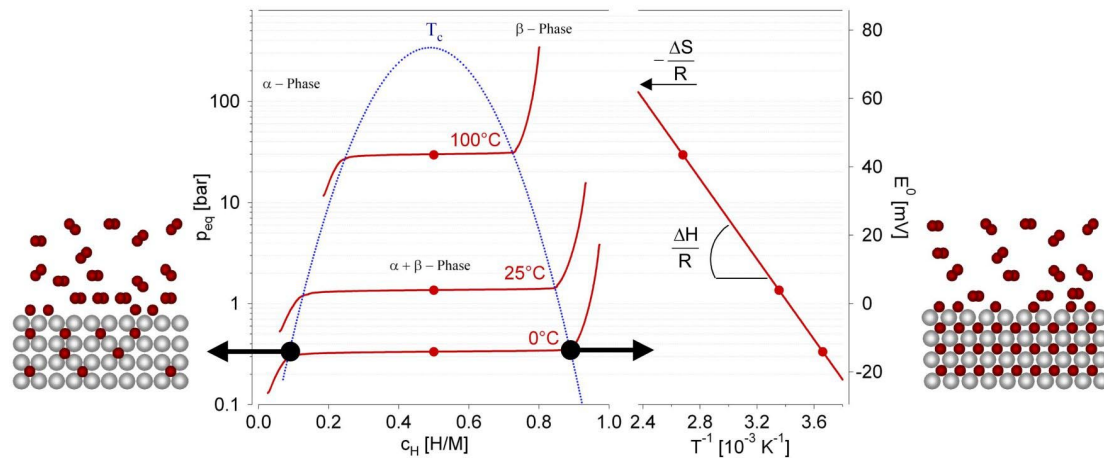


Fig. IX.13: Pressure composition isothermes for the hydrogen absorption in a typical intermetallic compound on the left hand side. The solid solution (α -phase), the hydride phase (β -phase) and the region of the coexistence of the two phases. The coexistange region is characterized by the flat plateau and ends at the critical temperature T_c . The construction of the Van't Hoff plot is shown on the right hand side. The slope of the line is equal to the enthalpy of formation divided by the gas constant and the interception is equal to the entropy of formation divided by the gas constant.

Several empirical models allow the estimation of the stability and the concentration of hydrogen in an intermetallic hydride. The maximum amount of hydrogen in the hydride phase is given by the number of interstitial sites in the intermetallic compound for which to following two criteria apply. The distance between two hydrogen atoms on interstitial sites is at least 2.1\AA [44] and the radius of the largest sphere on an interstitial site touching all the neighboring metallic atoms is at least 0.37\AA (Westlake criterion) [45]. The theoretical maximum volumetric density of hydrogen in a metal hydride, assuming a closed packing of the hydrogen, is therefore $253\text{ kg}\cdot\text{m}^{-3}$, which is 3.6 times the density of liquid hydrogen. As a general rule it can be stated, that all elements with an electronegativity in the range of 1.35 to 1.82 do not form stable hydrides [46]. Exemptions are Vanadium (1.45) and Chromium (1.56), which form hydrides and Molybdenum (1.30) and Technetium (1.36) where hydride formation would be expected. The adsorption enthalpy can be estimated from the local environment of the hydrogen atom on the interstitial site. According to the rule of imaginary binary hydrides the stability of a hydrogen on an interstitial site is the weighted average of the stability of the corresponding binary hydrides of the neighboring metallic atoms [47]. More general is the rule of reversed stability (Miedema model): The more stable a intermetallic compound the less stable is the corresponding hydride and the other way around.

[48]. This model is based on the fact that hydrogen can only participate on a bond with a neighboring metal atom if the bonds between the metal atoms are at least partially broken.

$$\Delta\bar{H}_\infty = a \cdot \Delta E \cdot \sqrt{W} \cdot \sum_j R_j^{-4} + b$$

$$a = 18.6 \text{ kJ} \cdot \text{mol}^{-1} \text{H} \text{Å}^4 \text{eV}^{-3/2}$$

$$b = -90 \text{ kJ} \cdot \text{mol}^{-1} \text{H}$$

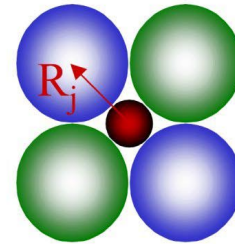
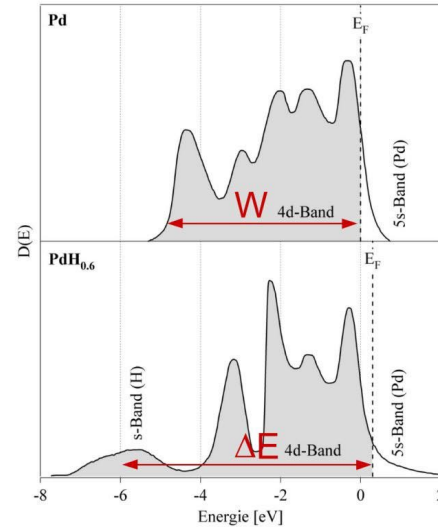
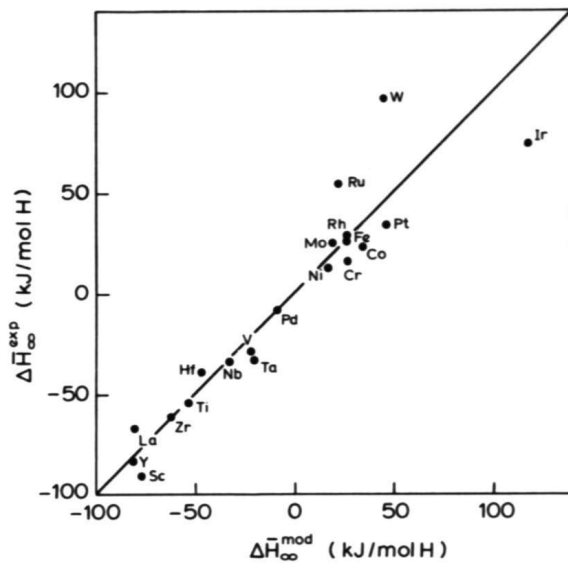


Fig. IX.14: The local band-structure model. Ref.: R. Griessen, Phys. Rev. B **38** (1988), pp.3690-3698

Hydrogen absorption is electronically an incorporation of electrons and protons into the electronic structure of the host lattice. The electrons have to fill empty states at the Fermi energy E_F while the protons lead to the hydrogen induced s-band approximately 4eV below the E_F (see Fig. IX.14). The heat of formation of binary hydrides MH_x is related linearly to the characteristic band energy parameter $\Delta E = E_F - E_s$, where E_F is the Fermi energy and E_s the center of the host metal electronic band with a strong s character at the interstitial sites occupied by hydrogen. For most metals E_s can be taken as the energy which corresponds to one electron per atom on the integrated density-of-states curve [49]. The semi-empirical models mentioned above allow an estimation of the stability of binary hydrides as long as the rigid band theory can be applied. However, the interaction of hydrogen with the electronic structure of the host metal in some binary hydrides and especially in the ternary hydrides is often more complicated. In many cases the crystal structure of the host metal and therefore, also the electronic structure changes upon the phase transition and the theoretical calculation of the stability of the hydride becomes very complicated if not presently impossible.

The stability of metal hydrides is usually presented in the form of Van't Hoff plots according to Eq.IX.7. Typical Van't Hoff plots are shown in Fig. IX.15 (see also Fig.III.24). The most stable binary hydrides have enthalpies of formation of $\Delta H_f = -113 \text{ kJ/molH}$ e.g. HoH_2 . The least stable hydrides are $\text{FeH}_{0.5}$, $\text{NiH}_{0.5}$ and $\text{MoH}_{0.5}$ with enthalpies of formation of $\Delta H_f = +10 \text{ kJ/molH}$, $\Delta H_f = +10 \text{ kJ/molH}$, and $\Delta H_f = +46 \text{ kJ/molH}$, respectively [50].

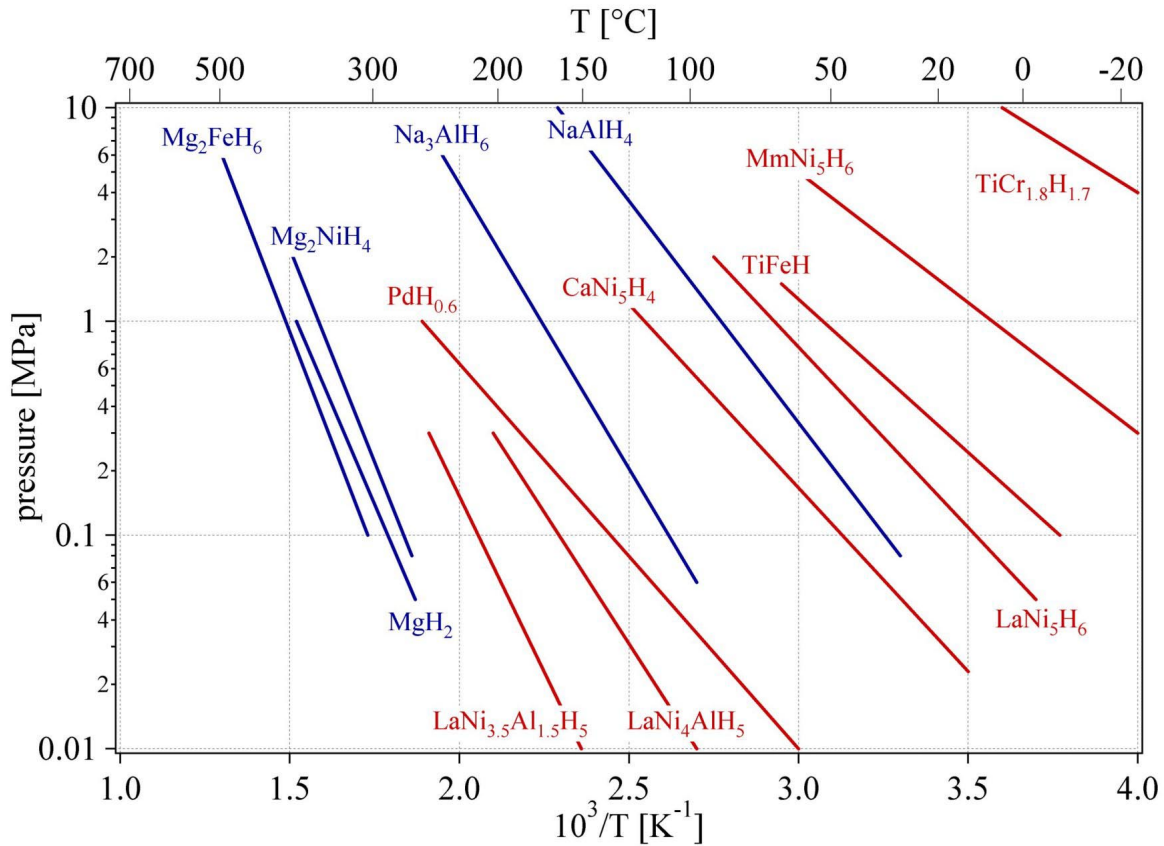


Fig. IX.15: Van't Hoff plots of some selected hydrides. The stabilisation of the hydride of LaNi_5 by the partial substitution of nickel with aluminum in LaNi_5 is shown as well as the substitution of lanthanum with mischmetal (e.g. 51% La, 33% Ce, 12% Nd, 4% Pr).

Due to the phase transition upon hydrogen absorption, metal-hydrides have the very useful property of absorbing large amounts of hydrogen at a constant pressure, i.e. the pressure does not increase with the amount of hydrogen absorbed as long as the phase transition takes place. The characteristics of the hydrogen absorption and desorption can be tailored by partial substitution of the constituent elements in the host lattice. Some metal hydrides absorb and desorb hydrogen at ambient temperature and close to atmospheric pressure. Several families of intermetallic compounds listed in Table IX.4 are interesting for hydrogen storage. They all consist of an element with a high affinity to hydrogen, the A-element, and an element with a low affinity to hydrogen, the B-element. The latter often involves nickel, since nickel is an excellent catalyst for the hydrogen dissociation.

One of the most interesting features of the metallic hydrides is the extremely high volumetric density of the hydrogen atoms present in the host lattice. The highest volumetric hydrogen density known today is 150 kg m^{-3} found in Mg_2FeH_6 and $\text{Al}(\text{BH}_4)_3$. Both hydrides belong to the complex hydrides and will be discussed in the next Section. Metallic hydrides reach a volumetric hydrogen density of 115 kg m^{-3} e.g. LaNi_5 . Most metallic hydrides absorb hydrogen up to a hydrogen to metal ratio of $\text{H/M} = 2$. Greater ratios up to $\text{H/M} = 4.5$ e.g. BaReH_9 , [51] have been found, however all hydrides with a hydrogen to metal ratio of more than 2 are ionic or covalent compounds and belong to the complex hydrides.

Metal hydrides are very effective to store large amounts of hydrogen in a safe and compact way. All the reversible hydrides working around ambient temperature and atmospheric pressure consist of transition metals; therefore the gravimetric hydrogen density is limited to less than 3 mass%. It is still a challenge to explore the properties of the light weight metal hydrides.

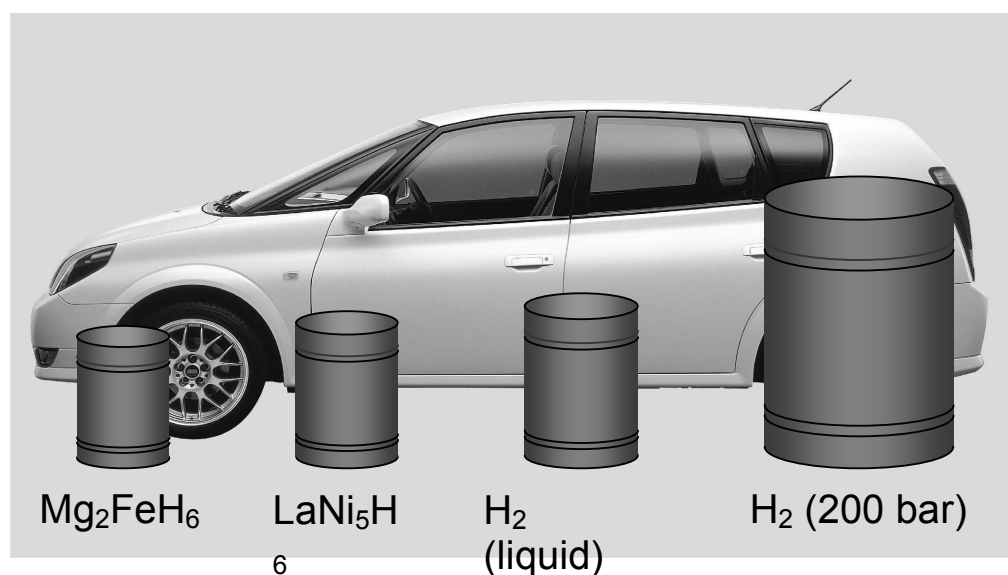


Fig. IX.16 : Volume required to store 4 kg of hydrogen of various systems.

IX.2.5 COMPLEX HYDRIDES

The group one two and three light elements, e.g. Li, Mg, B, Al, form a large variety of metal-hydrogen complexes. They are especially interesting because of their lightweight and the number of hydrogen atoms per metal atom which is in many cases 2. The main difference of the complex hydrides to the above described metallic hydrides is the transition to an ionic or covalent compound of the metals upon hydrogen absorption (see Chapter VII). Hydrogen in the complex

hydrides is often located at the corners of tetrahedrons with boron or aluminum at their centre. The negative charge of the anion, $[\text{BH}_4]^-$ and $[\text{AlH}_4]^-$ is compensated by a cation e.g. Li or Na. The hydride complexes of borane, the tetrahydroborates $\text{M}(\text{BH}_4)$, and of alane, the tetrahydroaluminate $\text{M}(\text{AlH}_4)$ are potentially interesting storage materials, although they were so far known to be stable and to decompose only at elevated temperatures and often above their melting point.

Bogdanovic and Swickardi [52] presented in 1996 for the first time adsorption and desorption pressure-concentration isotherms of catalyzed NaAlH_4 at temperature of 180°C and 210°C . The isotherms exhibit an absence of hysteresis and a nearly horizontal pressure plateau. Furthermore, the catalyzed system reversibly absorbed and desorbed hydrogen up to 4.2 mass% and the mechanism of the two step reaction was described. A more detailed study of the NaAlH_4 with an improved catalyst was published in 2000 by Bogdanovic et al. [53]. A desorption hydrogen pressure of 2 bar at 60°C was found and the enthalpy for the dissociation reaction was determined to be $37 \text{ kJ}\cdot\text{mol}^{-1}$ and $47 \text{ kJ}\cdot\text{mol}^{-1}$ for the first dissociation step of Ti-doped NaAlH_4 : $3 \text{ NaAlH}_4 \rightarrow \text{Na}_3\text{AlH}_6 + 2 \text{ Al} + 3 \text{ H}_2$ (3.7 wt% H) and the second $\text{Na}_3\text{AlH}_6 \rightarrow 3\text{NaH} + \text{Al} + 3/2 \text{ H}_2$ (3.0 wt% H), respectively. Therefore, the equilibrium hydrogen pressure at room temperature is approximately 1 bar. Furthermore, the reaction is reversible and a complete conversion to product was achieved at 270°C under 175 bar hydrogen pressure in 2-3 hours [54].

The first report of a pure alkali metal tetrahydroboride appeared in 1940 by Schlesinger and Brown [55] who synthesized the lithiumtetrahydroboride (lithiumborohydride) (LiBH_4) by the reaction of ethyllithium with diborane (B_2H_6). The direct reaction of the corresponding metal with diborane in etheral solvents under suitable conditions produces high yields of the tetrahydroborides [56] $2 \text{ MH} + \text{B}_2\text{H}_6 \rightarrow 2 \text{ MBH}_4$ where $\text{M} = \text{Li}, \text{Na}, \text{K}$ etc. Direct synthesis from the metal, boron and hydrogen at $550 - 700^\circ\text{C}$ and 30 - 150 bar H_2 has been reported to yield the lithium salt, and it has been claimed that such a method is generally applicable to groups IA and IIA metals [57]. The reaction involving either the metal or the metal hydride, or the metal together with triethylborane in an inert hydrocarbon has formed the basis of a patent $\text{M} + \text{B} + 2\text{H}_2 \rightarrow \text{MBH}_4$, where $\text{M} = \text{Li}, \text{Na}, \text{K}$ etc.

The stability of metal tetrahydroborides has been discussed in relation to their percentage ionic character, and those compounds with less ionic character than diborane are expected to be highly unstable [58]. Steric effects have also been suggested to be important in some compounds [59, 60]. The special feature exhibited by the covalent metal hydroborides is that the hydroboride group is bonded to the metal atom by bridging hydrogen atoms similar to the bonding in diborane, which may be regarded as the simplest of the so called "electron-deficient" molecules. Such molecules possess fewer electrons than those apparently required to fill all the bonding orbitals, based on the criterion that a normal bonding orbital involving two atoms contains two electrons. The molecular orbital bonding scheme for diborane is discussed extensively in [60].

The compound with the highest gravimetric hydrogen density at room temperature known today is LiBH_4 (18 mass%). Therefore, this complex hydride could be the ideal hydrogen storage material for mobile applications. LiBH_4 desorbs three of the four hydrogen in the compound upon melting at 280°C and decomposes into LiH and boron. The desorption process can be catalyzed by adding SiO_2 and significant thermal desorption was observed starting at 100°C [61]. Recently it has been shown, that the hydrogen desorption reaction is reversible and the end products lithium-hydride and boron absorb hydrogen at 690°C and 200 bar to form LiBH_4 [62]. The scientific understanding of the mechanism of the thermal hydrogen desorption from LiBH_4 and the absorption remains a challenge and more research work has to be carried out. Very little is known today about $\text{Al}(\text{BH}_4)_3$ a complex hydride with a very high gravimetric hydrogen density of 17

mass% and the highest known volumetric hydrogen density of $150 \text{ kg}\cdot\text{m}^{-3}$. Furthermore, $\text{Al}(\text{BH}_4)_3$ has a melting point of -65°C and is liquid at room temperature. Beside of the covalent hydrocarbons, this is the only liquid hydride at room temperature.

IX.2.6 CHEMICAL REACTION WITH WATER

Hydrogen can be generated from metals and chemical compounds reacting with water. The common experiment (demonstrated in many chemistry classes) where a piece of sodium floating on water produces hydrogen, demonstrates such a process. The sodium is transformed into sodium hydroxide in this reaction. The reaction is not directly reversible but the sodium hydroxide could later be removed and reduced in a solar furnace back to metallic sodium. Two sodium atoms react with two water molecules and produces one hydrogen molecule. The hydrogen molecule produces again a water molecule in the combustion, which can be recycled to generate more hydrogen gas. However, the second water molecule necessary for the oxidation of the two sodium atoms has to be added. Therefore, sodium has a gravimetric hydrogen density of 3 mass%. The same process carried out with lithium leads to a gravimetric hydrogen density of 6.3 mass%. The major challenge with this storage method is the reversibility and the control of the thermal reduction process in order to produce the metal in a solar furnace. The process has been successfully demonstrated with zinc [63]. The first, endothermic step is the thermal dissociation of $\text{ZnO}(\text{s})$ into $\text{Zn}(\text{g})$ and O_2 at 2300 K using concentrated solar energy as the source of process heat. The second, non-solar, exothermic step is the hydrolysis of $\text{Zn}(\text{l})$ at 700 K to form H_2 and $\text{ZnO}(\text{s})$; the latter separates naturally and is recycled to the first step. Hydrogen and oxygen are derived in different steps, thereby eliminating the need for high-temperature gas separation. A second-law analysis performed on the closed cyclic process indicates a maximum energy conversion efficiency of 29% (ratio of $\Delta G (\text{H}_2 + 0.5 \text{O}_2 \rightarrow \text{H}_2\text{O})$ for the H_2 produced to the solar power input), when using a solar cavity-receiver operated at 2300 K and subjected to a solar flux concentration ratio of 5000. The major sources of irreversibility are associated with the re-radiation losses from the solar reactor and the quenching of $\text{Zn}(\text{g})$ and O_2 to avoid their recombination. An economic assessment for a large-scale chemical plant, having a solar thermal power input into the solar reactor of 90 MW and a hydrogen production output from the hydrolyser of 61 GWh/year, indicates that the cost of solar hydrogen ranges between 0.13 and 0.15\$/kWh (based on its low heating value and a heliostat field cost at 100-150\$/ m^2) and, thus, might be competitive with other renewable-based routes such as electrolysis of water using solar-generated electricity. The economic feasibility of the proposed solar process is strongly dependent on the development of an effective Zn/O_2 separation technique (either by quench or by in situ electrolytic separation) that eliminates the need for an inert gas.

IX.2.7 SUMMARY HYDROGEN STORAGE

Hydrogen will be stored in various ways depending on the application e.g. mobile or stationary. Today we know several efficient and safe ways to store hydrogen, however there are many other new potential materials and methods possible to increase the hydrogen density significantly. The material science challenge is to better understand the electronic behavior of the interaction of hydrogen with other elements and especially metals. Complex compounds such $\text{Al}(\text{BH}_4)_3$ have to

be investigated and new compounds from the light weight metals and hydrogen will be discovered.

Based on today best technology a car powered with an internal combustion engine consumes 2.4 kg (3 liter) of gasoline per 100 km. Energetically this corresponds to 0.8 kg of hydrogen per 100 km. In order to drive the car for 500 km before refilling the hydrogen storage system, the car needs 4 kg of hydrogen on board. The tank with 4 kg hydrogen stored in a metal hydride is about 300 kg and has a volume of approximately 60 liter. Since such a storage vessel is mainly a steel compartment filled with a metallic powder it can be used as a constructive element of the car. In this case not all of the weight of the storage system is additional weight to the car. Furthermore, energy conversion devices more efficient than the internal combustion engine ,e.g. fuel cells, will be developed and reduce the amount of hydrogen necessary on board and therefore also the weight of the storage system.

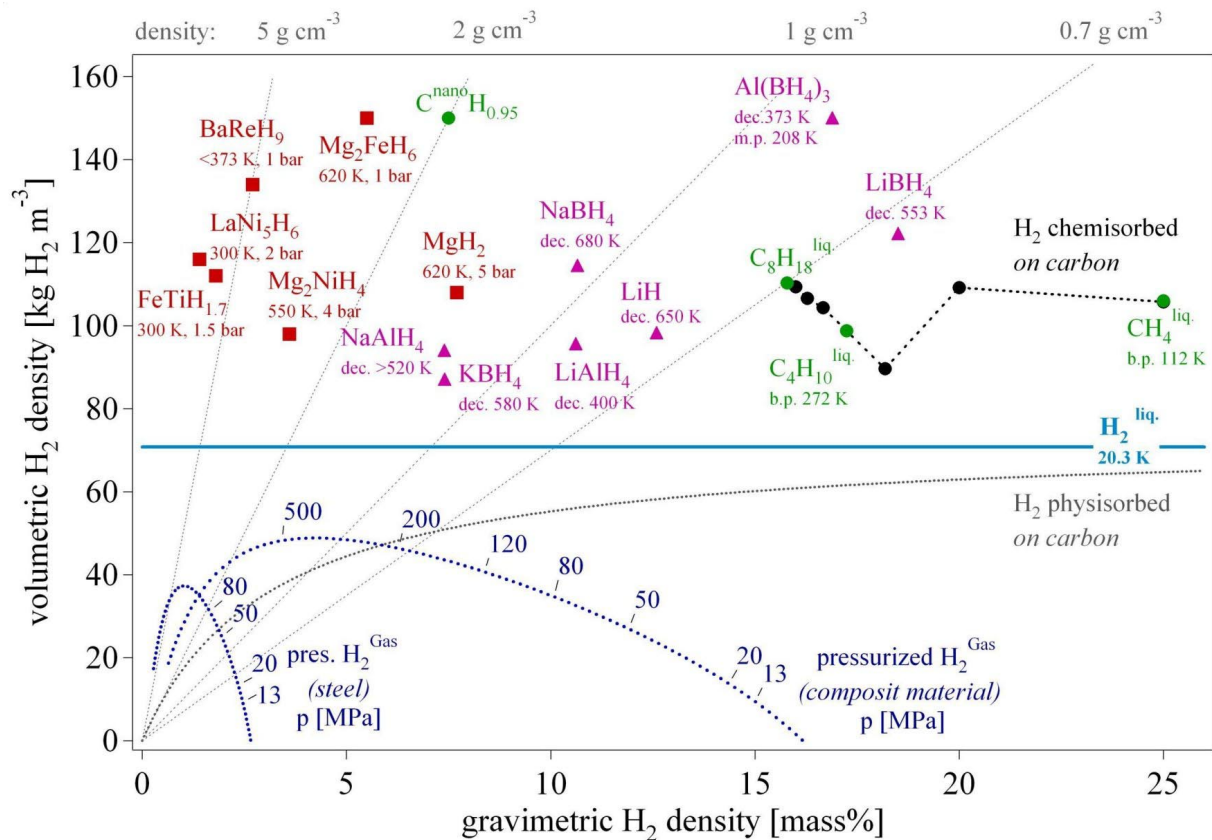
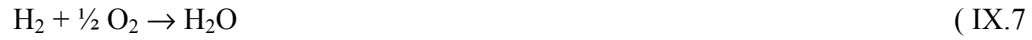


Fig. IX.17: Volumetric and gravimetric hydrogen density of some selected hydrides. Mg₂FeH₆ shows the highest known volumetric hydrogen density of 150 kg·m⁻³, which is more than the double of liquid hydrogen. BaReH₉ has the largest H/M ratio of 4.5, i.e. 4.5 hydrogen atoms per metal atom. LiBH₄ exhibits the highest gravimetric hydrogen density of 18 mass%. Pressurized gas storage is shown for steel (tensile strength σ_v = 460 MPa, density 6500 kg·m⁻³) and a hypothetical composite material (σ_v = 1500 MPa, density 3000 kg·m⁻³).

IX.3 ENERGY CONVERSION

The energy stored in hydrogen is liberated in the reaction of hydrogen with oxygen.



The enthalpy of formation of water is $\Delta H_f = -285 \text{ kJ}\cdot\text{mol}^{-1}$ at 25°C . Therefore, the upper heating value of hydrogen is $39.4 \text{ kWh}\cdot\text{kg}^{-1}$ [5]. The difference between the upper and the lower heating value is the enthalpy of vaporization of water ($\Delta H_v(\text{H}_2\text{O}) = 50 \text{ kJ}\cdot\text{mol}^{-1}$) according to the state of the water, liquid or vapor respectively, as a result of the combustion. For hydrogen the lower heating value is $33.3 \text{ kWh}\cdot\text{kg}^{-1}$.

The energy from the combustion can occur partially as work other than $p\cdot V$ i.e. electricity and as heat ($\Delta H_f = \Delta W_{\text{el.}} + \Delta Q = 39.4 \text{ kWh}\cdot\text{kg}^{-1}$). The maximum amount of work from the reaction is given by the Gibbs free energy ΔG_f :

$$\Delta G = \Delta H - T\Delta S \quad (\text{IX.8})$$

The entropy change for the hydrogen combustion and formation of liquid water is $\Delta S = -163 \text{ J}\cdot\text{K}^{-1}\cdot\text{mol}^{-1}$. The enthalpy is temperature dependent $dH/dT = c_p$.

The engines used to convert the chemical energy in a fuel to mechanical work are based on the combustion of the fuel with air and the use of the expansion of the gas delivering the work $p\cdot dV$. These engines e.g. steam engine (1712), Stirling engine (1816), Otto-motor (1863), Diesel-motor, Wankel-motor, and gas turbines, are based on a theoretical cycle described by Sadi Carnot (1824). The cycle consists of an isothermal and adiabatic expansion followed by a isothermal and adiabatic compression. The work extracted from the cycle is maximal when the entropy decrease in the hot heat reservoir (T_1) is equal to the entropy increase in the cold heat reservoir (T_2).

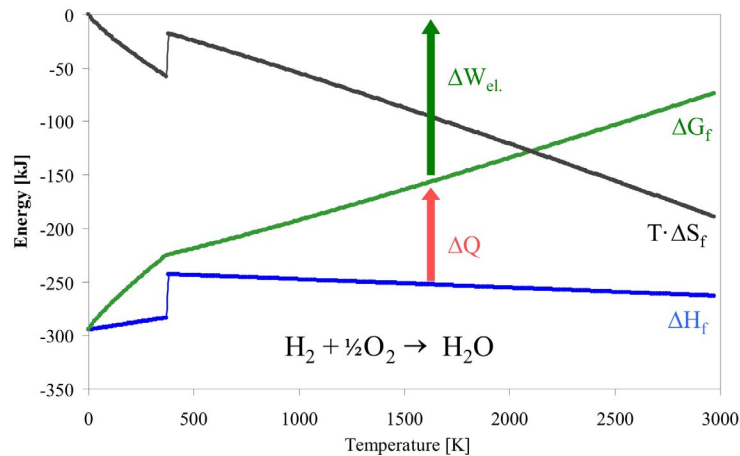


Fig. IX.18: Enthalpy ΔH , Heat $\Delta Q = T\Delta S$, and the Gibbs free energy ΔG as a function of temperature. The jumps in ΔS and ΔH are due to the vaporisation of water.

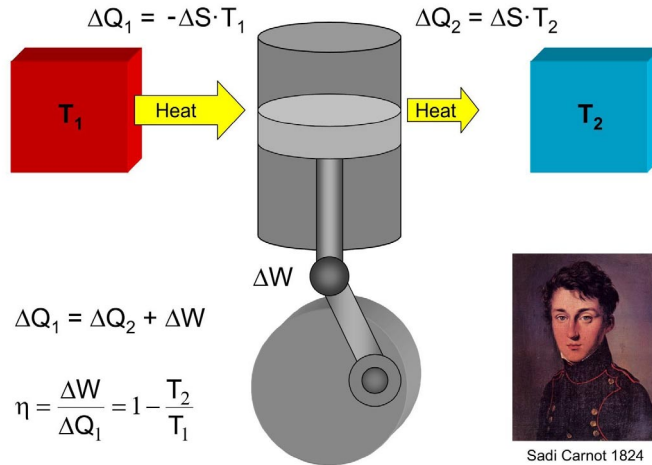


Fig. IX.19: Schematic representation of the Carnot cycle. Heat ΔQ_1 flows from the hot reservoir at the temperature T_1 into the Carnot machine which delivers the work ΔW . The heat ΔQ_2 flows then from the machine into the cold heat reservoir at the temperature T_2 .

According to the second law of thermodynamics is the entropy change in the Universe of the system equal to zero for a reversible process and greater than zero for all irreversible processes, i.e. $\Delta S_{Univ.} \geq 0$. The Carnot cycle describes the reversible process i.e. the physical limit of a working machine. The entropy increase in the cold reservoir is larger than the entropy decrease in the hot reservoir for all real machines.

The efficiency i.e. the ratio of work delivered by the machine to the amount of heat supplied, for the Carnot cycle is given by

$$\eta = \frac{\Delta W}{\Delta Q_1} = \frac{\Delta Q_1 - \Delta Q_2}{\Delta Q_1} = 1 - \frac{T_2}{T_1} \quad (\text{IX.9})$$

The efficiency of all real machines is therefore

$$\eta \leq 1 - \frac{T_2}{T_1} \quad (\text{IX.10})$$

and the temperatures T_1 is given by the maximum combustion temperature and T_2 by the temperature of the gas leaving the cylinder.

The reaction of hydrogen with oxygen can also take place as half reactions in an electrochemical cell.

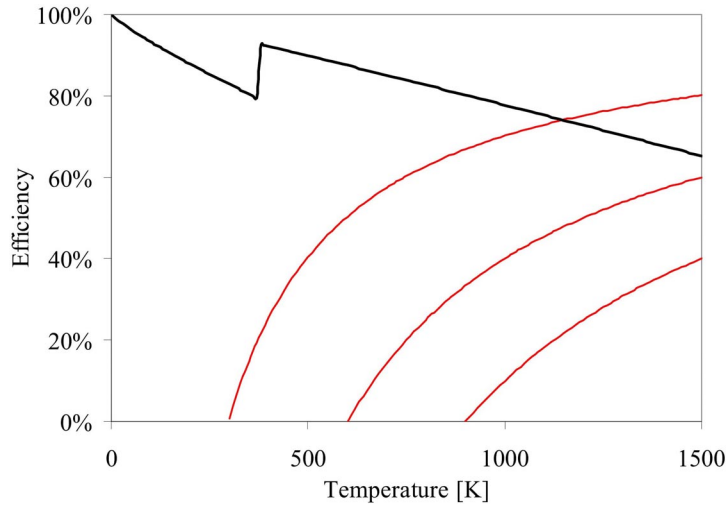
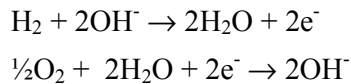


Fig. IX.20: Theoretical maximum efficiency of a fuel cell (black) as a function of temperature. The red lines represent Carnot efficiencies as a function of the temperature T_1 for $T_2 = 300, 600$ and 900 K. The jump in the fuel cell efficiency is due to the vaporisation of water.



The half reactions occur on separated electrodes, where an electrolyte allows the exchange of the OH^- ions. The potential built up between the two electrodes allows a current in the outer circuit and therefore, the electrochemical cell (alkaline fuel cell) delivers directly work as electricity. The open circuit potential ΔE of the cell is given by

$$\Delta G_f = -n \cdot F \cdot \Delta E \quad (\text{IX.11})$$

where n stands for the number of electrons transferred and F for the Faraday constant ($F = 96484.56 \text{ Cmol}^{-1}$). Therefore, the theoretical maximum efficiency of the fuel cell at constant temperature is given by

$$\eta = \frac{\Delta G_f}{\Delta H_f} = 1 - T \cdot \frac{\Delta S_f}{\Delta H_f} \quad (\text{IX.12})$$

The interesting conclusion is here that the theoretical efficiency of a fuel cell can greatly exceed that of a Carnot machine. Diesel engines reach today an efficiency of 40%. It is assumed that low temperature fuel cell systems could reach 65% of efficiency. In the Appendix we show that the Heliocentris demonstration fuel cell has an efficiency between 35 and 50% depending on the load.

IX.4 VISIONS FOR THE FUTURE

Hydrogen is likely to be the synthetic fuel for the future because of the large heating value and the possibility to produce it from renewable energy in a closed cycle (water-hydrogen-water). The conversion of the energy stored in hydrogen into work is theoretically more efficient using a fuel cell than an internal combustion engine. Therefore the mobile energy consumption could be reduced by approximately 35% with the introduction of fuel cells. The introduction of hydrogen as a synthetic fuel is, however, independent of the fuel cells. Just like fossil fuels have started the industrial age, hydrogen will start an economic and technical revolution. Once the investments for the production of renewable energy are carried out mankind will profit from a hydrogen based environmentally clean energy economy.

IX.5 CONCLUSION

The hydrogen revolution following the industrial age has just started. Hydrogen production, storage and conversion has reached a technological level although plenty of improvements and new discoveries are still expected. The hydrogen storage is often considered as the bottleneck of the renewable energy economy based on the synthetic fuel hydrogen. Six different hydrogen storage methods have been described. In addition to the well established high pressure cylinders for laboratory applications and the liquid hydrogen for air and space applications, metal hydrides and complex hydrides offer a very safe and efficient way to store hydrogen. Further scientific research and technical developments will lead to new materials with a higher volumetric and gravimetric hydrogen density. The best materials today show a volumetric storage density of $150 \text{ kg}\cdot\text{m}^{-3}$ which can be improved by approximately 50% according to theoretical estimates.

Within the large “Sustainable Hydrogen” National Program the VU group is actively developing new methods for the fast screening of potentially attractive new and lightweight storage materials.

IX.6 REFERENCES

- [1] S. S. Wilson, *Spektrum der Wissenschaft* (Oktober 1981), pp. 99-109
- [2] *Bulletin, Magazin der Eidgenössischen Technischen Hochschule Zürich* 276 (2000)
- [3] *Climate Change 2001: Synthesis Report*, Robert T. Watson (ed.), Published for the Intergovernmental Panel on Climate Change IPCC, (2001), Cambridge University Press, Cambridge, UK
- [4] International Energy Agency (IEA, AIE), “Key World Energy Statistics” 2002 Edition.
- [5] *Handbook of Chemistry and Physics*, Weast R. C., ed. 57 (1976), CRC Press
- [6] Steinfeld A., Palumbo R., “Solar Thermochemical Process Technology”, *Encyclopedia of Physical Science and Technology*, R. A. Meyers Ed., Academic Press 15 (2001), pp. 237-256, ISBN 0-12-227410-5.
- [7] Product specification from GTec SA, rte de Clos-Donroux 1, CH-1870 Monthey, Switzerland.
- [8] Huston, E.L., „ALiquid and Solid Storage of Hydrogen.“ *Proceedings of the 5th World Hydrogen Energy Conference*. Vol. 3; July 15-20, 1984, Toronto, Canada
- [9] Flynn, T.M., „A Liquefaction of Gases.“ *McGraw-Hill Encyclopedia of Science & Technology*. 7th edition. Vol. 10. New York: McGraw-Hill; (1992).pp. 106-109.
- [10] Gary Chen and Samim Anghaie based on NASA/NIST databases, http://www.inspi.ufl.edu/data/h_prop_package.html
- [11] M. von Ardenne, G. Musiol, S. Reball, “Effekte der Physik”, Verlag Harry Deutsch (1990), pp. 712-715
- [12] F. London, *Z. Physik*. 63 (1930), pp. 245; *Z. Physik. Chem.* 11 (1930), pp. 222
- [13] S. Brunauer, P.H. Emmett and E. Teller, *J. Amer. Chem. Soc.* 60 (1938), pp. 309.
- [14] A.C. Dillon, K.M. Jones, T.A. Bekkedahl, C.H. Kiang, D.S. Bethune, and M.J. Heben, *Nature* 386 (1997), p. 377.

- [15] A. C. Dillon et al. Proceedings of the 2000 DOE/NREL hydrogen program review, May 8-10, (2000)
- [16] M. Hirscher, M. Becher, M. Haluska, U. Dettlaff-Weglikowska, A. Quintel, G.S. Duesberg, Y.M. Choi, P. Downes, M. Hulman, S. Roth, I. Stepanek, P. Bernier, *Applied Physics A* 72 (2001), p. 129.
- [17] S.J. Gregg and K.S.W. Sing, "Adsorption, Surface Area and Porosity", Academic Press (1967), London and New York
- [18] G. Stan and M. W. Cole, *Low Temperature Physics* 100 (1998), p. 539.
- [19] M. Rzepka, P. Lamp, and M.A. de la Casa-Lillo, *J. of Phys. Chem. B* 102 (1998), p. 10849.
- [20] K. A. Williams and P. C. Eklund, *Chemical Physics Letters* 320 (2000), p. 352.
- [21] S.M. Lee, K.H. An, Y.H. Lee, G. Seifert, T. Frauenheim, *J. Korean Phys. Soc.* 38 (2001), p. 686; S.M. Lee and Y.H. Lee, *Appl. Phys. Lett.* 76 (2000), p. 2879.
- [22] Y. Ma, Y. Xia, M. Zhao, R. Wang, and L. Mei, *Phys. Rev. B* 63 (2001), p. 115422.
- [23] W. B. Leung and N. H. March, and H. Motz, *Physics Letters* 56 (1976), p. 425.
- [24] R.A. Beebe, J. Bischoe, W.R. Smith, and C.B. Wendell, *J. Am. Chem. Soc.* 69 (1947), p. 95.
- [25] A. Züttel, P. Sudan, Ph. Mauron, T. Kyiobaiashi, Ch. Emmenegger, and L. Schlapbach, *Int. J. of Hydrogen Energy* 27 (2002), p. 203.
- [26] Y. Ye, C.C. Ahn, C. Witham, B. Fultz, J. Liu, A.G. Rinzler, D. Colbert, K.A. Smith, and R.E. Smalley, *Appl. Phys. Letters* 74 (1999), p. 2307.
- [27] C. Liu, Y.Y. Fan, M. Liu, H.T. Cong, H.M. Cheng, M.S. Dresselhaus, *Science*, 286 (1999), p. 1127.
- [28] Y.Y. Fan, B. Liao, M. Liu, Y.L. Wei, M.Q. Lu, and H.M. Cheng, *Carbon*, 37 (1999), p. 1649.
- [29] P. Chen, X. Wu, J. Lin, and K.L. Tan, *Science* 285 (1999), p. 91.
- [30] M. Hirscher, M. Becher, M. Haluska, A. Quintel, V. Skakalova, Y.M. Choi, U. Dettlaff-Weglikowska, S. Roth, I. Stepanek, P. Bernier, A. Leonhardt, and J. Fink, *J. of Alloys and Compounds* 330-332 (2002), p. 654.
- [31] R. Ströbel, L. Jörisen, T. Schliermann, V. Trapp, W. Schütz, K. Bohmhammel, G. Wolf, and J. Garche, *J. of Power Sources* 84 (1999), p. 221.
- [32] M.G. Nijkamp, J.E.M.J. Raaymakers, A.J. van Dillen, and K.P. de Jong, *Appl. Phys. A* 72 (2001), p. 619.
- [33] Ch. Nützenadel, A. Züttel, and L. Schlapbach, Chap. 9 "Electronic Properties of Novel Materials", *Science and Technology of Molecular Nanostructures*, eds. H. Kuzmany, J. Fink, M. Mehring, and S. Roth, American Institute of Physics, New York (1999), p. 462
- [34] Ch. Nützenadel, A. Züttel, Ch. Emmenegger, P. Sudan, and L. Schlapbach, Chap. 10 "Sciences and Applications of Nanotubes", *Kluwer Academic Publishing / Plenum Press, "Fundamental Materials Research Series"*, Ed. M. F. Thorpe, p. 205
- [35] A. Züttel, P. Sudan, Ph. Mauron, Ch. Emmenegger, T. Kiyobayashi, and L. Schlapbach, *J. of Metastable and Nanocrystalline Materials* 11 (2001) p. 95.
- [36] S.M. Lee, K.S. Park, Y.C. Choi, Y.S. Park, J.M. Bok, D.J. Bae, K.S. Nahm, Y.G. Choi, S.Ch. Yu, N. Kim, T. Frauenheim, and Y.H. Lee, *Synthetic Metals* 113 (2000), p. 209.
- [37] Weitkamp J; Fritz M; Ernst S, *International J. of Hydrogen Energy*, Vol. 20, Nr. 12 (1995), pp. 967-970
- [38] Langmi H W; Walton A; Al-Mamouri M M; Johnson S R, Book D; Speight J D; Edwards P P; Gameson I; Anderson P A; Harris I R, *J. of Alloys and Compounds* in press (2003)
- [39] N. L. Rosi, J. Eckert, M. Eddaoudi, D. T. Vodak, J. Kim, M. O'Keeffe, O. M. Yaghi, *Science* 300 (2003), pp. 1127-1129.
- [40] G. R. Pearson, *Chem. Rev.* 85 (1985) 41-49.
- [41] W. M. Mueller, I. R. Blackledge, G. G. Libowitz (eds.): *Metal Hydrides*, Academic Press, New York (1968)
- [42] J. E. Lennard-Jones, *Trans. Faraday Soc.* 28 (1932), pp. 333
- [43] Y. Fukai, *Z. Phys. Chem.* 164 (1989), pp. 165
- [44] A. C. Switendick, *Z. Phys. Chem. N.F.* 117 (1979), pp. 89
- [45] D.J. Westlake, *J. Less-Common Metals* 91 (1983), pp.275-292
- [46] Peter Rittmeyer, Ulrich Wietelmann, "Chap.: Hydrides", *Ullmann's Encyclopedia of Industrial Chemistry*, Fifth, Completely Revised Edition, Volume A13: High-Performance Fibers to Imidazole and Derivatives, VCH, pp. 199-226
- [47] A. R. Miedema, *J. Less-Common Met* 32 (1973), pp. 117
- [48] H. H. Van Mal, K.H.J. Buschow and A.R. Miedema, *J. Less-Com. Met.* 35 (1974), pp. 65
- [49] R. Griessen and A. Driessen, *Phys. Rev. B* 30:8 (1984), pp. 4372-4381
- [50] R. Griessen and T. Riesterer, "Heat of Formation Models" in "Hydrogen in Intermetallic Compounds I Electronic, Thermodynamic, and Crystallographic Properties, Preparation", L. Schlapbach, ed., *Springer Series Topics in Applied Physics*, Vol. 63 (1988), pp. 219-284.
- [51] Klaus Yvon, "Complex Transition Metal Hydrides ", *Chimia* 52:10 (1998), pp. 613-619
- [52] B. Bogdanovic, M. Schwickardi, *J. Alloys Comp.* 253-254 (1997), pp. 1-9
- [53] B. Bogdanovic, R.A. Brand, A. Marjanovic, M. Schwickardi, J. Tolle, *J. of Alloys and Compounds*, 2000, Vol 302, Iss 1-2, pp 36-58
- [54] T. N. Dymova, N.G. Eliseeva, S. I. Bakum, Y. M. Dergachev, *Dok. Akad. Nauk USSR* 215 (1974), pp. 1369

- [55] H. J. Schlesinger and H. C. Brown, *J. American Chemical Society* 62 (1940), pp. 3429-3435.
- [56] H. J. Schlesinger, H. C. Brown, H. R. Hoekstra, L. R. Rapp, *J. of the American Chemical Society* 75 (5 JAN 1953), pp. 199-204
- [57] D. Goerrig, *Ger. Pat.* 1,077,644 (Dec. 27, 1958)
- [58] G. N. Schrauzer, *Naturwissenschaften* 42 (1955), pp. 438
- [59] S. J. Lippard and D. A. Ucko, *Inorg. Chem.* 7 (1968), pp. 1051
- [60] W. N. Lipscomb, *Boron Hydrides*, Benjamin, New York (1963)
- [61] Züttel A; Wenger P; Rensch S; Sudan P; Mauron P; Emmenegger C, *J. of Power Sources* 5194 (2003), pp.1-7
- [62] P. Sudan, A. Züttel...*Letter to Nature* (2003)
- [63] A. Steinfeld, *International J. of Hydrogen Energy* 27 (2002), pp. 611 –619